

# On seismic ambient noise cross-correlation and surface-wave attenuation

Lapo Boschi<sup>1,2</sup>, Fabrizio Magrini<sup>3</sup>, Fabio Cammarano<sup>3</sup>, and Mark van der Meijde<sup>4</sup>

<sup>1</sup>Dipartimento di Geoscienze, Università degli Studi di Padova, Italy

<sup>2</sup>Sorbonne Université, CNRS, INSU, Institut des Sciences de la Terre de Paris, ISTE P UMR 7193, F-75005 Paris, France.

<sup>3</sup>Department of Geological Science, Università degli Studi Roma Tre, Italy

<sup>4</sup>Faculty of Geo-Information Science and Earth Observation (ITC), University of Twente, The Netherlands

July 11, 2019

## Summary

We derive a theoretical relationship between the cross correlation of ambient Rayleigh waves (seismic ambient noise) and the attenuation parameter  $\alpha$  associated with Rayleigh-wave propagation. In particular, we derive a mathematical expression for the multiplicative factor relating normalized cross correlation to the Rayleigh-wave Green's function. Based on this expression, we formulate an inverse problem to determine  $\alpha$  from cross correlations of recorded ambient signal. We conduct a preliminary application of our algorithm to a relatively small instrument array, conveniently deployed on an island. In our setup, the mentioned multiplicative factor has values of about 2.5 to 3, which, if neglected, could result in a significant underestimate of  $\alpha$ . We find that our inferred values of  $\alpha$  are reasonable, in comparison with independently obtained estimates found in the literature. Allowing  $\alpha$  to vary with respect to frequency results in a reduction of misfit between observed and predicted cross correlations.

## 1 Introduction

A number of theoretical and experimental studies have proved that the cross correlation between two recordings of a diffuse surface-wave field approximately coincides with the surface-wave Green's function associated with the two points of observation. This is relevant to the field of seismology, since recorded seismic ambient signal has been found to mostly consist of seismic surface waves, and empirical Green's functions are now routinely retrieved from the cross correlation of seismic ambient noise [e.g. *Boschi and Weemstra, 2015*, and references therein]. Most authors have been able to derive the medium's velocity from the *phase* of the reconstructed Green's functions; this resulted in successful applications of ambient-noise theory to imaging and monitoring [see the reviews by, e.g., *Campillo and Roux, 2014*; *Boschi*

33 *and Weemstra, 2015*]. The *amplitude* of the Green’s function in principle provides comple-  
34 mentary information on the medium’s anelastic properties; but it tends to be less accurately  
35 reconstructed by cross correlation.

36 Initial attempts to constrain surface-wave attenuation from ambient noise [e.g. *Prieto*  
37 *et al., 2009*; *Harmon et al., 2010*; *Lawrence and Prieto, 2011*; *Weemstra et al., 2013*] were  
38 based on the assumption (questioned by *Weaver [2011]*) that the “lossy” Green’s func-  
39 tion be simply the product of the elastic Green’s function times an exponential damping  
40 term. *Tsai [2011]* validated mathematically this assumption, but both he and *Harmon et al.*  
41 [2010] emphasized the difficulty of constraining earth’s attenuation whenever the ambient  
42 field is not perfectly diffuse. The study of *Weemstra et al. [2014]* additionally showed that  
43 data-processing techniques typically used in ambient-noise literature, such as whitening or  
44 time-domain normalization [e.g. *Bensen et al., 2007*], could also affect attenuation estimates.  
45 Whitening and/or normalization, however, are necessary to avoid that localized events of  
46 relatively large amplitude, like earthquakes, obscure random noise and thus bias cross corre-  
47 lations.

48 It is the purpose of this study to introduce a new normalization criterion, which is in prac-  
49 tice similar to whitening, but is derived directly from the reciprocity theorem as stated, e.g.,  
50 by *Boschi and Weemstra [2015]*; i.e., it does not follow from data-processing considerations,  
51 but from the physics of ambient-noise cross correlation. The relationship we obtain (eq. (30)  
52 in sec. 2.3.2), and on whose basis we formulate an inverse problem to determine attenuation,  
53 can be summarized simplistically by stating that cross correlations are normalized against the  
54 power spectral density of emitted noise. An approximate equation expressing source power  
55 spectral density in terms of recorded data is also found (eqs. (27) and (29), sec. 2.3.2). To  
56 achieve all this, we assume the same theoretical framework of, e.g., *Boschi et al. [2018]*, de-  
57 scribing Love- and Rayleigh-wave as combinations of two-dimensional membrane waves and  
58 “radial eigenfunctions.” Our treatment (sec. 2) involves an independent derivation of the  
59 surface-wave Green’s function in a lossy medium (sec. 2.1 and app. B).

60 Importantly, the fact that the medium is lossy requires that noise sources be uniformly  
61 distributed over the surface of the earth (and not just over all azimuths) for the Green’s  
62 function to be reconstructed by noise cross-correlation [*Snieder, 2007*; *Tsai, 2011*]. In addi-  
63 tion, our formulation is strictly valid only if the spectrum of signal emitted by ambient-noise  
64 sources is laterally homogeneous (sec. 2.3). Because seismic ambient noise is mostly origi-  
65 nated by coupling between the solid earth and the oceans, it is reasonable to expect that  
66 both requirements will be best approximated by deploying instruments on an island. We ac-  
67 cordingly test our algorithm on two years of continuous data recorded by an array of fourteen  
68 broadband stations in Sardinia. We explore two different parameterizations of attenuation in  
69 the area of interest, i.e. constant (sec. 3.2.1) vs. frequency-dependent (sec. 3.2.2) attenuation  
70 parameter. In both cases, we identify an attenuation model that minimizes data misfit. We  
71 discuss the resulting models in light of independent studies of Rayleigh-wave attenuation.

## 72 2 Theory

### 73 2.1 Green's problem for a lossy membrane

74 Let us first summarize the treatment of surface-wave theory given by *Boschi et al.* [2018],  
 75 based on earlier studies by *Tanimoto* [1990] and *Tromp and Dahlen* [1993]. We shall work  
 76 in the frequency ( $\omega$ ) domain and employ the Fourier-transform convention of *Boschi and*  
 77 *Weemstra* [2015]. It is convenient to first introduce the Rayleigh- ( $\mathbf{u}_R$ ) and Love-wave ( $\mathbf{u}_L$ )  
 78 displacement *Ansätze*

$$\mathbf{u}_R(x_1, x_2, x_3, \omega) = U(x_3, \omega)\mathbf{x}_3\phi_R(x_1, x_2, \omega) + V(x_3, \omega)\nabla_1\phi_R(x_1, x_2, \omega), \quad (1)$$

$$\mathbf{u}_L(x_1, x_2, x_3, \omega) = W(x_3, \omega)(-\mathbf{x}_3 \times \nabla_1)\phi_L(x_1, x_2, \omega), \quad (2)$$

79  
 80 respectively, where  $x_1, x_2, x_3$  are Cartesian coordinates, with the  $x_3$ -axis perpendicular to  
 81 Earth's surface (which we assume to be flat) and oriented downward; the unit-vectors  $\mathbf{x}_1, \mathbf{x}_2,$   
 82  $\mathbf{x}_3$  are parallel to the Cartesian axes;  $\nabla_1$  denotes the surface gradient  $\mathbf{x}_1\frac{\partial}{\partial x_1} + \mathbf{x}_2\frac{\partial}{\partial x_2}$ . The  
 83 functions  $U(x_3, \omega), V(x_3, \omega)$  and  $W(x_3, \omega)$  control the dependence of surface-wave amplitude  
 84 on depth, and the functions  $\phi_R(x, \omega)$  and  $\phi_L(x, \omega)$  are respectively dubbed Rayleigh- and  
 85 Love-wave "potentials". Upon substituting expressions (1) and (2) into the frequency-domain  
 86 displacement equation, it is found that  $\phi_R$  and  $\phi_L$  can be determined through the Helmholtz'  
 87 equations

$$\nabla_1^2\phi_{L,R}(x_1, x_2, \omega) + \frac{\omega^2}{c_{L,R}^2}\phi_{L,R}(x_1, x_2, \omega) = f(x_1, x_2, \omega), \quad (3)$$

88 where  $c_{L,R}(\omega)$  denote the value of Rayleigh- or Love-wave phase velocity at frequency  $\omega$  and  
 89  $f$  is a generic forcing term.

90 This study is limited to recordings of seismic ambient noise. Because seismic noise has  
 91 been shown to essentially amount to surface waves, it is safe (provided that signals related to  
 92 large or nearby earthquakes are excluded) to assume that eqs. (1) and (2) correctly describe  
 93 the corresponding ground displacement. Furthermore, for the sake of simplicity we only  
 94 consider vertical-component recordings, i.e., the  $\mathbf{x}_3$ -component of  $\mathbf{u}_R$ , or

$$u_{R,3} = U(0, \omega)\phi_R(x_1, x_2, \omega), \quad (4)$$

95 with  $x_3=0$  as long as recordings are made at Earth's surface. It is inferred upon multiplying  
 96 eq. (3) by  $U(0, \omega)$  that the following vertical-displacement equation holds,

$$\nabla_1^2u_{R,3}(x_1, x_2, \omega) + \frac{\omega^2}{c_R^2}u_{R,3}(x_1, x_2, \omega) = U(0, \omega)f(x_1, x_2, \omega). \quad (5)$$

97 Eqs. (3) and (5) coincide with the equation governing the displacement of a lossless,  
 98 stretched membrane [e.g. *Kinsler et al.*, 1999]. Following *Boschi and Weemstra* [2015], we  
 99 define the Green's function  $G_{2D}$  as the membrane response to impulsive (Dirac  $\delta(x_1)\delta(x_2)$ )  
 100 initial velocity at the reference-frame origin, with zero initial displacement and zero forcing  
 101 term  $f$ ; it follows (app. A.1) that, for Rayleigh waves,

$$G_{2D}(x_1, x_2, \omega) = -\frac{iP}{4\sqrt{2\pi}c_R^2}H_0^{(2)}\left(\frac{\omega x}{c_R}\right), \quad (6)$$

102 where  $i$  denotes the imaginary unit,  $H_0^{(2)}$  the zeroth-order Hankel function of the second kind  
 103 [e.g. *Abramowitz and Stegun*, 1964, eq. (9.1.4)],  $P$  accounts for the physical dimensions of  
 104  $G_{2D}$  as discussed in app. A.1, and  $x = \sqrt{x_1^2 + x_2^2}$  is the distance between  $(x_1, x_2)$  and the  
 105 “source.”

106 Following *Tsai* [2011], we now make the assumption that surface-wave attenuation can  
 107 be accounted for by replacing eq. (5) with a *damped* membrane equation, i.e. introducing  
 108 an additional forcing term, or “loss term proportional to, and oppositely directed from, the  
 109 velocity of the vibrating element” [*Kinsler et al.*, 1999, sec. 4.6]. It is convenient to denote  
 110  $\frac{2\alpha}{c_R}$  the proportionality factor between force and velocity, with the “attenuation coefficient”  
 111  $\alpha$  coinciding with that of *Tsai* [2011]. In the frequency domain, the resulting displacement  
 112 equation reads

$$\nabla_1^2 u(x_1, x_2, \omega) + \left( \frac{\omega^2}{c^2} - i \frac{2\alpha\omega}{c} \right) u(x_1, x_2, \omega) = U(0, \omega) f(x_1, x_2, \omega) \quad (7)$$

113 [e.g. *Kinsler et al.*, 1999; *Tsai*, 2011], where all unnecessary subscripts have been dropped.  
 114 It is inferred by comparing eqs. (5) and (7) that the expression (6) is still a solution of (7),  
 115 if the real ratio  $\omega/c$  in its argument is replaced by the complex number  $\sqrt{\frac{\omega^2}{c^2} - \frac{2i\alpha\omega}{c}}$  [*Kinsler*  
 116 *et al.*, 1999; *Snieder*, 2007; *Tsai*, 2011; *Weemstra et al.*, 2015]; the two-dimensional, *damped*  
 117 Green’s function therefore reads

$$G_{2D}^d(x_1, x_2, \omega) = -\frac{iP}{4\sqrt{2\pi}c^2} H_0^{(2)} \left( x \sqrt{\frac{\omega^2}{c^2} - \frac{2i\alpha\omega}{c}} \right). \quad (8)$$

118 We show in app. B that as long as attenuation is relatively weak, i.e.  $\alpha \ll \omega/c$  [*Tsai*,  
 119 2011], and provided that frequency is high and/or the effects of near-field sources are negli-  
 120 gible, expression (8) can be reduced to the more convenient, approximate form

$$\begin{aligned} G_{2D}^d(x_1, x_2, \omega) &\approx -\frac{iP}{4\sqrt{2\pi}c^2} H_0^{(2)} \left( \frac{\omega x}{c} \right) e^{-\alpha x} \\ &\approx G_{2D}(x_1, x_2, \omega) e^{-\alpha x}; \end{aligned} \quad (9)$$

121 in other words, if  $\frac{\omega x}{c} \gg 1$  and  $\alpha \ll \omega/c$ , the lossy-membrane Green’s function  $G_{2D}^d$  can be  
 122 roughly approximated by the product of the lossless two-dimensional Green’s function  $G_{2D}$   
 123 times a damping term  $e^{-\alpha x}$ ; we verified this result via numerical tests (Fig. 1).

## 124 2.2 Reciprocity theorem for a lossy membrane

125 We extend the reciprocity-theorem derivation of *Boschi et al.* [2018], who only considered  
 126 lossless media, to the case of a lossy membrane. The procedure that follows is similar to that  
 127 of *Snieder* [2007], which, however, is limited to lossy *three-dimensional* media. In analogy  
 128 with *Boschi et al.* [2018], let us introduce a vector  $\mathbf{v} = -\frac{1}{i\omega} \nabla_1 u$ , such that

$$\nabla_1 u + i\omega \mathbf{v} = \mathbf{0}. \quad (10)$$

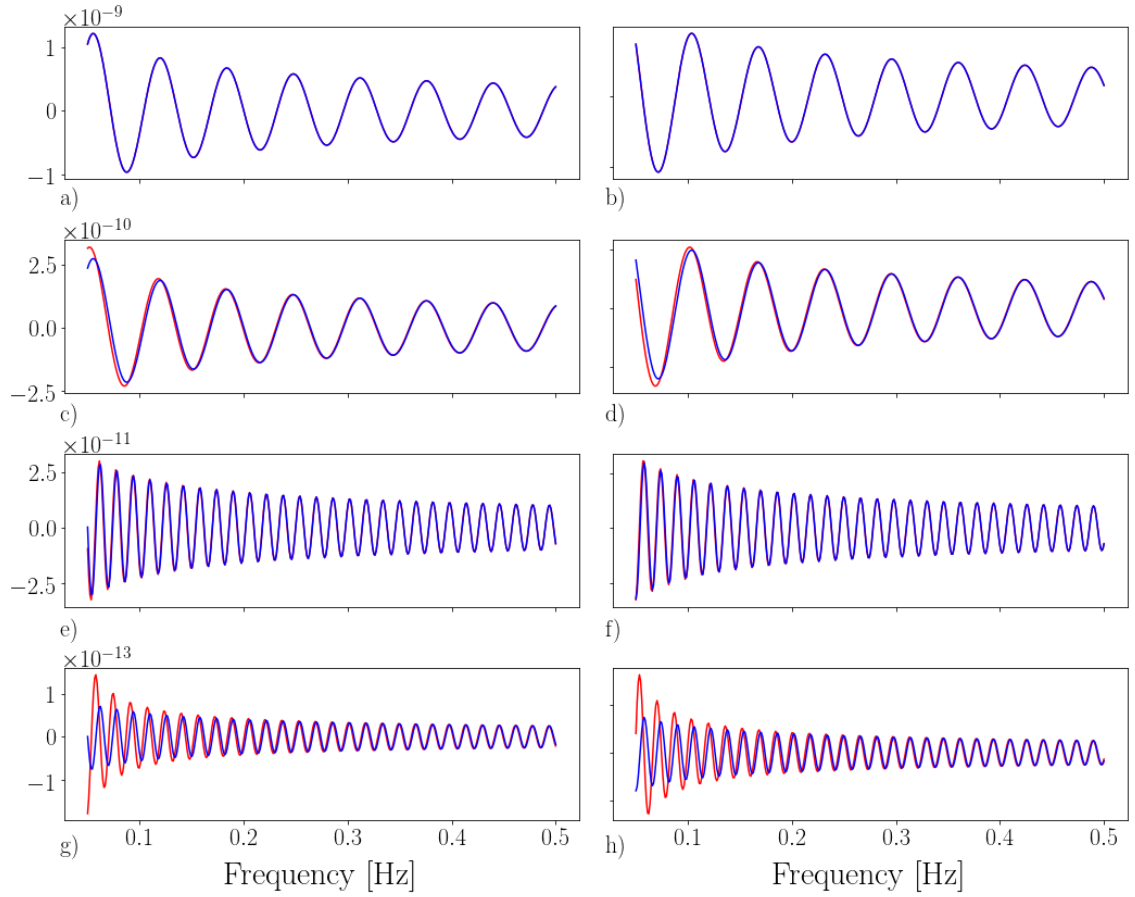


Figure 1: Comparison between the exact (red) and approximate (blue) formulae (eqs. (8) and (9), respectively) for the lossy-membrane Green's function. The real parts of the Green's function are shown on the left (panels a, c, e, g), the imaginary parts on the right (b, d, f and h). Green's functions corresponding to interstation distances of 50 km (a through d) and 200 km (e through h), and  $\alpha=2 \times 10^{-5}\text{m}^{-1}$  (a, b, e and f) and  $\alpha=5 \times 10^{-5}\text{m}^{-1}$  (c, d, g and h) are shown. The approximation is good when  $\alpha$  is small and  $\omega$  is high, and decays with growing  $\alpha$  and decreasing  $\omega$ .

129 Upon substituting (10) into the damped-membrane displacement equation (7),

$$\nabla_1 \cdot (-i\omega \mathbf{v}) + \left( \frac{\omega^2}{c^2} - i \frac{2\alpha\omega}{c} \right) u = U(0, \omega) f. \quad (11)$$

130 After some algebra,

$$\nabla_1 \cdot \mathbf{v} + i \frac{\omega\kappa}{c^2} u - q = 0, \quad (12)$$

131 where  $\kappa = 1 - i \frac{2\alpha c}{\omega}$  for brevity, and  $q = \frac{i}{\omega} U(0, \omega) f$  to be consistent with *Boschi et al.* [2018].  
 132 In the frequency domain,  $q$  has units of squared time over distance. (*Kinsler et al.* [1999]  
 133 show that, in the stretched-membrane model, this forcing can be thought of as proportional  
 134 to “pressure divided by surface density”.)

135 Eqs. (10) and (12) are similar to eqs. (24) and (25) of *Boschi et al.* [2018], except that  
 136 the real number  $\frac{\omega}{c^2}$  in eq. (25) of *Boschi et al.* [2018] is replaced here by the complex  $\frac{\omega\kappa}{c^2}$ .

137 Following *Boschi et al.* [2018], consider an area  $S$  on the membrane, bounded by the closed  
 138 curve  $\partial S$ ; let  $q_A(x_1, x_2, \omega)$ ,  $u_A(x_1, x_2, \omega)$  and  $\mathbf{v}_A(x_1, x_2, \omega)$  denote a possible combination of  
 139 the fields  $q$ ,  $p$  and  $\mathbf{v}$  co-existing at  $(x_1, x_2)$  in  $S$  and  $\partial S$ . A different forcing  $q_B$  would  
 140 give rise, through eqs. (10) and (12), to a different “state”  $B$ , defined by  $u_B(x_1, x_2, \omega)$  and  
 141  $\mathbf{v}_B(x_1, x_2, \omega)$ . The reciprocity theorem is obtained by combining the left-hand sides of eqs.  
 142 (10) and (12) as follows,

$$\int_S d^2 \mathbf{x} [(10)_A \cdot \mathbf{v}_B^* + (10)_B^* \cdot \mathbf{v}_A + (12)_A u_B^* + (12)_B^* u_A] = 0, \quad (13)$$

143 where  $\mathbf{x} = (x_1, x_2)$ ,  $d^2 \mathbf{x} = dx_1 dx_2$ , and  $*$  denotes complex conjugation.  $(10)_A$  is short for the  
 144 expression one obtains after substituting  $u = u_A(\mathbf{x}, \omega)$  and  $\mathbf{v} = \mathbf{v}_A(\mathbf{x}, \omega)$  into the left-hand  
 145 side of eq. (10), etc. Following the same procedure as in sec. 3 of *Boschi et al.* [2018], we  
 146 find

$$\int_S d^2 \mathbf{x} [\nabla_1 (u_A \cdot \mathbf{v}_B^*) + \nabla_1 (u_B^* \cdot \mathbf{v}_A)] + \frac{i\omega}{c^2} (\kappa - \kappa^*) \int_S d^2 \mathbf{x} u_A u_B^* = \int_S d^2 \mathbf{x} (q_A u_B^* + q_B^* u_A). \quad (14)$$

147 Notice that the second term at the left-hand side of eq. (14) would be 0 if the membrane  
 148 were lossless ( $\alpha=0$ , and therefore  $\kappa=\kappa^*$ ); it is easy to see that in that case (14) is equivalent  
 149 eq. (31) of *Boschi et al.* [2018].

150 The divergence theorem allows to reduce the first surface integral at the left-hand side  
 151 of (14) to a line integral along  $\partial S$ . Following *Snieder* [2007], we consider the particular  
 152 case where surface integration is over the entire two-dimensional space  $\mathbb{R}^2$ , i.e. the area  $S$   
 153 is infinite. This is relevant to seismic ambient-noise applications, where receiver arrays are  
 154 typically deployed within a relatively small area, receiving signal from “noise” sources that  
 155 are distributed with (approximately) equal probability over the entire surface of the globe.  
 156 Then, for attenuating media the wave field vanishes exponentially at infinity, and the integral  
 157 along  $\partial S$  accordingly vanishes. We are left with

$$\frac{4\alpha}{c} \int_{\mathbb{R}^2} d^2 \mathbf{x} u_A u_B^* = \int_{\mathbb{R}^2} d^2 \mathbf{x} (q_A u_B^* + q_B^* u_A). \quad (15)$$

158 Consider now the states  $A$  and  $B$  associated with impulsive forcing terms  $q_A = F\delta(\mathbf{x} - \mathbf{x}_A)$   
 159 and  $q_B = F\delta(\mathbf{x} - \mathbf{x}_B)$ , respectively.  $\mathbf{x}_A$  and  $\mathbf{x}_B$  are two arbitrary point-source locations, and

160 the factor  $F$  accounts for the physical dimensions of  $q$  (recall that  $\delta(\mathbf{x})$  has dimensions of one  
 161 over squared distance). It follows from app. A, eq. (A.22), that the corresponding membrane  
 162 displacements are  $u_A = i\omega \frac{Fc^2}{P} G_{2D}^d(\mathbf{x}, \mathbf{x}_A, \omega)$  and  $u_B = i\omega \frac{Fc^2}{P} G_{2D}^d(\mathbf{x}, \mathbf{x}_B, \omega)$ , respectively.  
 163 Substituting into eq. (15),  $F$  simplifies out and

$$\frac{2\alpha\omega c}{P} \int_{\mathbb{R}^2} d^2\mathbf{x} G_{2D}^d(\mathbf{x}, \mathbf{x}_A, \omega) G_{2D}^{d*}(\mathbf{x}, \mathbf{x}_B, \omega) = -\Im[G_{2D}^d(\mathbf{x}_A, \mathbf{x}_B, \omega)], \quad (16)$$

164 which is the sought reciprocity theorem. Eq. (16) is similar, e.g., to eq. (39) of *Boschi*  
 165 *et al.* [2018], with one fundamental difference: the integral in (16) is not over a closed curve  
 166 containing the receiver pair (as in *Boschi et al.* [2018]), but over the entire real plane. As  
 167 shown in the following, this implies that, for the *lossy* Green’s function  $G_{2D}^d$  to be accurately  
 168 reconstructed by seismic interferometry, sources should be uniformly distributed over space,  
 169 rather than azimuth, and both in the near and far field of the receivers [*Snieder*, 2007; *Tsai*,  
 170 2011; *Weemstra et al.*, 2015].

## 171 2.3 Cross-correlation amplitude as a constraint for attenuation

172 We shall next (sec. 2.3.1) use eq. (16) to establish a relationship between the cross correlation  
 173 of ambient surface-wave signal (“noise”) recorded at two locations  $\mathbf{x}_A, \mathbf{x}_B$ , and the imaginary  
 174 part of the Green’s function  $G_{2D}^d(\mathbf{x}_A, \mathbf{x}_B, \omega)$ . Based on this relationship, in sec. 2.3.2 an  
 175 inverse problem will be formulated, having attenuation  $\alpha$  as unknown parameter, and the  
 176 cross correlation of recorded noise as data. In this endeavour, it is assumed that ambient noise  
 177 can be represented by a distribution of point sources of constant spatial density, emitting  
 178 at random times (i.e., random phase in the frequency domain) but, in analogy with the  
 179 numerical study of *Cupillard and Capdeville* [2010], all sharing the same spectral amplitude.  
 180 The assumption that the spectral amplitude of noise sources be constant across the globe  
 181 is based on the idea that Rayleigh-wave noise on earth is generated by the coupling, at the  
 182 ocean bottom, between oceans and the solid earth. It has been shown that, while local effects  
 183 play a role, the resulting spectrum has maxima determined by the main frequencies of ocean  
 184 waves (i.e., primary and secondary microseisms at 0.05–0.12 and 0.1–0.25 Hz, respectively),  
 185 independent of location [e.g. *Longuet-Higgins*, 1950; *Ardhuin et al.*, 2011; *Hillers et al.*, 2012].  
 186 We accordingly consider our assumption to be valid at least as a rough approximation of the  
 187 real world.

### 188 2.3.1 Noise cross-correlation and the Green’s function

189 The vertical-component, Rayleigh-wave displacement associated with a noise “event” can  
 190 be thought of as the time-domain convolution of  $G_{2D}^d$  and a source time function. In the  
 191 frequency domain, convolution is replaced by product, and the signal emitted at a point  $\mathbf{x}$   
 192 and recorded at, say, receiver  $\mathbf{x}_A$  reads  $h(\omega)G_{2D}^d(\mathbf{x}_A, \mathbf{x}, \omega)e^{i\omega\phi}$ , with  $h(\omega)$  and  $\phi$  denoting the  
 193 amplitude and phase of the emitted signal. It follows that the ambient noise recorded at  $\mathbf{x}_A$   
 194 can be written

$$s(\mathbf{x}_A, \omega) = h(\omega) \sum_{j=1}^{N_S} G_{2D}^d(\mathbf{x}_A, \mathbf{x}_j, \omega) e^{i\omega\phi_j}, \quad (17)$$

195 where  $N_S$  denotes the total number of sources, and the index  $j$  identifies the source; as an-  
 196 ticipated, it is assumed that the unitless, frequency-domain amplitude  $h(\omega)$  is approximately  
 197 the same for all noise sources. Based on eq. (17), the cross correlation of noise recorded at  
 198 two receivers  $\mathbf{x}_A, \mathbf{x}_B$  can be written

$$\begin{aligned}
 s(\mathbf{x}_A, \omega)s^*(\mathbf{x}_B, \omega) &= |h(\omega)|^2 \left[ \sum_{j=1}^{N_S} G_{2D}^d(\mathbf{x}_A, \mathbf{x}_j, \omega) e^{i\omega\phi_j} \right] \left[ \sum_{k=1}^{N_S} G_{2D}^{d*}(\mathbf{x}_B, \mathbf{x}_k, \omega) e^{-i\omega\phi_k} \right] \\
 &= |h(\omega)|^2 \left[ \sum_{j=1}^{N_S} G_{2D}^d(\mathbf{x}_A, \mathbf{x}_j, \omega) G_{2D}^{d*}(\mathbf{x}_B, \mathbf{x}_j, \omega) \right. \\
 &\quad \left. + \sum_{j=1}^{N_S} \sum_{k=1, k \neq j}^{N_S} G_{2D}^d(\mathbf{x}_A, \mathbf{x}_j, \omega) G_{2D}^{d*}(\mathbf{x}_B, \mathbf{x}_k, \omega) e^{i\omega(\phi_j - \phi_k)} \right]. \tag{18}
 \end{aligned}$$

199 The phases  $\phi_1, \phi_2, \phi_3, \dots$  are assumed to be random (uniformly distributed between 0 and  
 200  $2\pi$ ); it follows that the cross correlations of signals emitted by different sources, i.e. the second  
 201 term at the right-hand side of (18) (“cross terms”), can be neglected if noise is recorded over  
 202 a sufficiently long time, or if a sufficiently large amount of uniformly distributed sources are  
 203 present [e.g. *Weemstra et al.*, 2014; *Boschi and Weemstra*, 2015, App. D]; then

$$s(\mathbf{x}_A, \omega)s^*(\mathbf{x}_B, \omega) \approx |h(\omega)|^2 \sum_{j=1}^{N_S} G_{2D}^d(\mathbf{x}_A, \mathbf{x}_j, \omega) G_{2D}^{d*}(\mathbf{x}_B, \mathbf{x}_j, \omega). \tag{19}$$

204 It is convenient to transform the sum at the right-hand side of eq. (19) into an integral; said  
 205  $\rho$  the surface density of noise sources, which we assume to be constant,

$$s(\mathbf{x}_A, \omega)s^*(\mathbf{x}_B, \omega) \approx \rho |h(\omega)|^2 \int_{\mathbb{R}^2} d^2\mathbf{x} G_{2D}^d(\mathbf{x}_A, \mathbf{x}, \omega) G_{2D}^{d*}(\mathbf{x}_B, \mathbf{x}, \omega). \tag{20}$$

206 It will be noticed that the integral in (20) is over the entire real plane: this follows from the  
 207 assumption, made in sec. 2.1, that sources be uniformly distributed over  $\mathbb{R}^2$ . Dividing both  
 208 sides by  $\rho|h(\omega)|^2$ , we find from eq. (20) that

$$\int_{\mathbb{R}^2} d^2\mathbf{x} G_{2D}^d(\mathbf{x}_A, \mathbf{x}, \omega) G_{2D}^{d*}(\mathbf{x}_B, \mathbf{x}, \omega) \approx \frac{1}{\rho|h(\omega)|^2} s(\mathbf{x}_A, \omega)s^*(\mathbf{x}_B, \omega), \tag{21}$$

209 and finally, substituting eq. (21) into (16),

$$s(\mathbf{x}_A, \omega)s^*(\mathbf{x}_B, \omega) \approx -\frac{|h(\omega)|^2 P \rho}{2\alpha\omega c} \Im[G_{2D}^d(\mathbf{x}_A, \mathbf{x}_B, \omega)]. \tag{22}$$

210 Eq. (22) is the “lossy” counterpart of, e.g., eq. (65) of *Boschi and Weemstra* [2015].  
 211 Let us emphasize, again, that eq. (22) was obtained under the assumption that sources are  
 212 uniformly distributed over the entire real plane  $\mathbb{R}^2$ . It follows from eq. (22) that, in the  
 213 absence of attenuation, i.e.  $\alpha=0$ , the cross correlation of ambient signal at its left-hand side  
 214 is divergent. This is why in ambient-noise literature, whenever attenuation is neglected, the  
 215 assumption is made that sources are uniformly distributed with respect to *azimuth*, rather  
 216 than in space: for instance, the mentioned eq. (65) of *Boschi and Weemstra* [2015] results  
 217 from a uniform distribution of sources along a circle that surrounds the receivers.

218 Like eq. (65) of *Boschi and Weemstra* [2015], eq. (22) can be used as the basis of inverse  
 219 problems: the seismic observations at its left-hand side are “inverted” to constrain unknown  
 220 parameters contained in the theoretical formula at its right-hand side. Importantly, surface-  
 221 wave phase velocity  $c(\omega)$  can be determined from eq. (22) without knowledge of the factor  
 222  $|h(\omega)|^2 P\rho$  (that is to say, of the power spectral density, surface density and intensity of the  
 223 noise sources); *Ekström et al.* [2009] show that this amounts to identifying the values of  $c$  and  
 224  $\omega$  for which the left-hand side of eq. (22) is zero (i.e., the “zero crossings” of the reconstructed  
 225 Green’s function). The factor  $|h(\omega)|^2 P\rho$  becomes relevant if the Green’s function’s amplitude  
 226 is to be accurately reconstructed, which is necessary if one wants to determine attenuation.

### 227 2.3.2 From noise cross-correlation to attenuation: the inverse problem

228 We show in the following how eq. (22) can be manipulated to formulate an inverse problem  
 229 with  $\alpha$  as unknown parameter, without neglecting  $|h(\omega)|^2 P\rho$ . Let us start by expressing  
 230  $|h(\omega)|^2$  as a function of noise data.

231 It follows from eq. (17) that the power spectral density of the ambient signal recorded at  
 232 a location  $\mathbf{x}$  can be written

$$\begin{aligned}
 |s(\mathbf{x}, \omega)|^2 &= |h(\omega)|^2 \left[ \sum_{j=1}^{N_S} G_{2D}^d(\mathbf{x}, \mathbf{x}_j, \omega) e^{i\omega\phi_j} \right] \left[ \sum_{k=1}^{N_S} G_{2D}^{d*}(\mathbf{x}, \mathbf{x}_k, \omega) e^{-i\omega\phi_k} \right] \\
 &= |h(\omega)|^2 \left[ \sum_{j=1}^{N_S} |G_{2D}^d(\mathbf{x}, \mathbf{x}_j, \omega)|^2 + \sum_{j=1}^{N_S} \sum_{k=1, k \neq j}^{N_S} G_{2D}^d(\mathbf{x}, \mathbf{x}_j, \omega) G_{2D}^{d*}(\mathbf{x}, \mathbf{x}_k, \omega) e^{i\omega(\phi_j - \phi_k)} \right];
 \end{aligned}
 \tag{23}$$

233 then, if one neglects cross terms based on the same arguments as above,

$$\begin{aligned}
 |s(\mathbf{x}, \omega)|^2 &\approx |h(\omega)|^2 \sum_{j=1}^{N_S} |G_{2D}^d(\mathbf{x}, \mathbf{x}_j, \omega)|^2 \\
 &\approx |h(\omega)|^2 \sum_{j=1}^{N_S} |G_{2D}^d(r_j, \omega)|^2,
 \end{aligned}
 \tag{24}$$

234 where we have introduced the source-receiver distance  $r_j = |\mathbf{x} - \mathbf{x}_j|$ , to emphasize the fact that  
 235 the value of  $G_{2D}^d$  at a given point depends on its distance from the source, but not on the  
 236 absolute locations of source and receiver. We next transform the sum at the right-hand side  
 237 of eq. (24) into an integral over source-receiver distance; let us first replace the summation  
 238 over sources with a summation over  $N_D$  distance bins, i.e.,

$$|s(\mathbf{x}, \omega)|^2 \approx |h(\omega)|^2 \sum_{k=1}^{N_D} N_k |G_{2D}^d(r_k, \omega)|^2,
 \tag{25}$$

239 where  $N_k$  denotes the number of sources at distances between  $r_k$  and  $r_{k+1}$  from the receiver,  
 240 and it is assumed that  $G_{2D}^d(r_k, \omega) \approx G_{2D}^d(r, \omega)$  as long as  $r_k \leq r \leq r_{k+1}$  (which will be the  
 241 case as long as the increment  $\delta r = r_{k+1} - r_k$  is small). The area of the annulus centered at the  
 242 receiver and bounded by the circles of radii  $r_k$  and  $r_{k+1}$  is approximately  $2\pi r_k \delta r$ . It follows

243 that  $N_k \approx 2\pi r_k \rho \delta r$ , and

$$\begin{aligned}
|s(\mathbf{x}, \omega)|^2 &\approx 2\pi\rho|h(\omega)|^2 \sum_{k=1}^{N_D} \delta r r_k |G_{2D}^d(r_k, \omega)|^2 \\
&\approx 2\pi\rho|h(\omega)|^2 \int_0^\infty dr r |G_{2D}^d(r, \omega)|^2 \\
&\approx \frac{\rho P^2 |h(\omega)|^2}{16c^4} \int_0^\infty dr r \left| H_0^{(2)}\left(\frac{\omega r}{c}\right) \right|^2 e^{-2\alpha r},
\end{aligned} \tag{26}$$

244 where we have replaced  $G_{2D}^d$  with its leading term, according to eq. (9). We have not been  
245 able to find a closed-form solution for the integral at the right-hand side of eq. (26); let us  
246 denote

$$I(\alpha, \omega, c) = \int_0^\infty dr r \left| H_0^{(2)}\left(\frac{\omega r}{c}\right) \right|^2 e^{-2\alpha r}. \tag{27}$$

247 Then, solving eq. (26) for  $|h(\omega)|^2$ ,

$$|h(\omega)|^2 \approx \frac{16c^4}{\rho P^2 I(\alpha, \omega, c)} |s(\mathbf{x}, \omega)|^2. \tag{28}$$

248 Eq. (28) stipulates that the power-spectral density of emitted ambient noise can be obtained  
249 from the power-spectral density of signal recorded at any receiver  $\mathbf{x}$ , by application of a  
250 simple filter (provided that the surface density  $\rho$  and “intensity”  $P$  of noise sources are  
251 known). Since it was assumed that the function  $h$  is the same for all source-receiver vectors  
252  $\mathbf{x}$ , the right-hand side of (28) can be replaced by an average over all available receivers, which  
253 we denote  $\langle |s(\mathbf{x}, \omega)|^2 \rangle_{\mathbf{x}}$ :

$$|h(\omega)|^2 \approx \frac{16c^4}{\rho P^2 I(\alpha, \omega, c)} \langle |s(\mathbf{x}, \omega)|^2 \rangle_{\mathbf{x}}; \tag{29}$$

254 this is irrelevant from a purely theoretical perspective, but useful when processing real data,  
255 as averaging over all receivers will reduce effects that are not accounted for in our theoretical  
256 formulation, i.e. structural heterogeneities, dependence of the source time function on source  
257 location, nonuniformities in noise source distribution, etc.

258 Substituting (29) into (22), we find after some algebra that

$$\frac{s(\mathbf{x}_A, \omega) s^*(\mathbf{x}_B, \omega)}{\langle |s(\mathbf{x}, \omega)|^2 \rangle_{\mathbf{x}}} \approx \frac{c}{\omega I(\alpha, \omega, c)} \sqrt{\frac{2}{\pi}} J_0\left(\frac{\omega |\mathbf{x}_A - \mathbf{x}_B|}{c}\right) \frac{e^{-\alpha |\mathbf{x}_A - \mathbf{x}_B|}}{\alpha}, \tag{30}$$

259 where  $J_0$  denotes the zeroth-order Bessel function of the first kind [e.g. *Boschi and Weemstra,*  
260 *2015*]; importantly, the intensity  $P$  and surface density  $\rho$  of noise sources have canceled  
261 out, and only  $\alpha$  and  $c$  remain to be determined. A nonlinear inverse problem can then be  
262 formulated, with  $\alpha$  as its only unknown parameter. In practice, the dispersion curve  $c(\omega)$  is  
263 first inverted for, ideally through a robust method that bypasses amplitude information and  
264 only accounts for phase [e.g. *Ekström et al., 2009; Kästle et al., 2016*]. We discuss in sec. 3.2  
265 how a cost function to be minimized can then be introduced, based on eq. (30).

266 It might be noticed that a closed-form expression for  $\alpha$  can be derived from the above  
267 treatment. Let us rewrite eq. (30) after replacing  $\mathbf{x}_A$  and  $\mathbf{x}_B$  with the locations of two  
268 other stations in our array, denoted  $\mathbf{x}_C$  and  $\mathbf{x}_D$ . We next divide eq. (30) by the equation so

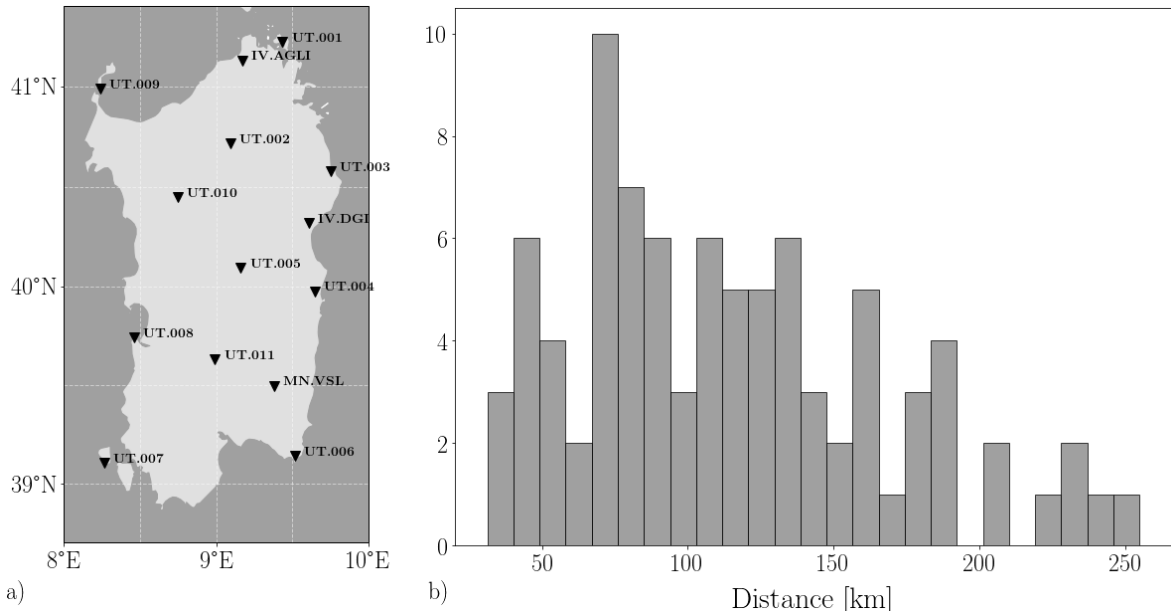


Figure 2: (a) Geographical locations of receivers (black triangles with station names) over the island of Sardinia. (b) Distribution of interstation distances for all station pairs in our deployment; the mean and median of the distribution are 114.45 km, 104.95 km, respectively. Acronyms starting with the letters UT identify stations deployed by our team.

269 obtained, and find

$$\frac{s(\mathbf{x}_A, \omega) s^*(\mathbf{x}_B, \omega)}{s(\mathbf{x}_C, \omega) s^*(\mathbf{x}_D, \omega)} \approx \frac{J_0(\omega |\mathbf{x}_A - \mathbf{x}_B|/c)}{J_0(\omega |\mathbf{x}_C - \mathbf{x}_D|/c)} e^{\alpha(|\mathbf{x}_C - \mathbf{x}_D| - |\mathbf{x}_A - \mathbf{x}_B|)}, \quad (31)$$

270 which can be solved for  $\alpha$  to obtain the sought formula

$$\alpha(\omega) = \log \left\{ \frac{[s(\mathbf{x}_A, \omega) s^*(\mathbf{x}_B, \omega)] [J_0(\omega |\mathbf{x}_C - \mathbf{x}_D|/c)]}{[s(\mathbf{x}_C, \omega) s^*(\mathbf{x}_D, \omega)] [J_0(\omega |\mathbf{x}_A - \mathbf{x}_B|/c)]} \right\} \frac{1}{|\mathbf{x}_C - \mathbf{x}_D| - |\mathbf{x}_A - \mathbf{x}_B|}, \quad (32)$$

271 where  $\log$  denotes the natural logarithm. We have found that application of eq. (32) to our  
 272 database does not lead to stable results, and, at the present stage, have not pursued this  
 273 approach further. Eq. (32) might be of interest in the presence of a more diffuse ambient  
 274 field, or a higher number of receivers allowing, e.g., for averaging over different azimuths as  
 275 in *Prieto et al.* [2009].

### 276 3 Application to Sardinian data set

277 At the end of June, 2016, our team has deployed an array of broadband seismic stations (Tril-  
 278 lium Nanometrics 120s posthole broadband stations) around Sardinia, as shown in Fig. 2a.  
 279 This temporary deployment was complemented by three permanent stations belonging to the  
 280 Italian MN and IV networks. Except for UT001 and UT011, stations recorded continuously  
 281 for 24 months. Station UT001 recorded from June 2016 until November 2017; it was then  
 282 removed and redeployed at location UT011, where it recorded November 2017 to September  
 283 2018. We next explain how ambient recordings of displacement (vertical component only)  
 284 were cross correlated to one another, to determine first a set of Rayleigh-wave dispersion  
 285 curves, and then, according to sec. 2.3.2, the attenuation parameter  $\alpha$ .

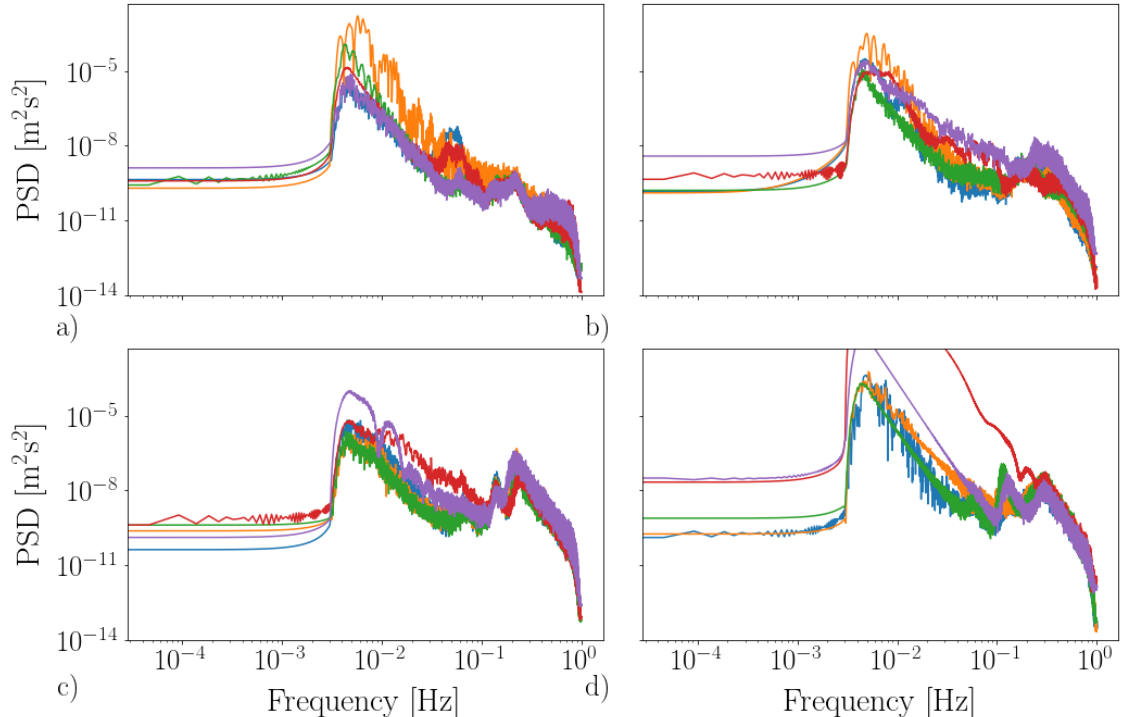


Figure 3: Five examples of power spectral density  $\langle |s(\mathbf{x}, \omega)|^2 \rangle_{\mathbf{x}}$ , computed for five consecutive six-hour long intervals. The computation is repeated for each season, with panels a, b, c and d showing the results obtained in summer, autumn, winter and spring, respectively. Recordings used for this examples start on (a) July 8, 2017 at 8:49AM; (b) October 5, 2017, at 2:49AM; (c) January 20, 2018, at 2:49AM; April 14, 2018, at 8:49PM.

### 286 3.1 Data cross correlation

287 Recordings of earthquakes are characterized by amplitudes much larger than those of truly  
 288 diffuse, “ambient” signal, and can accordingly bias cross correlations [e.g., *Bensen et al.*,  
 289 2007]. After subdividing seismic recordings into relatively short time intervals, some au-  
 290 thors minimize this bias by identifying intervals where anomalously large displacements are  
 291 recorded, to then exclude them from cross correlation. An alternative solution consists of  
 292 cross-correlating separately the segments of seismic recording associated with each time inter-  
 293 val; then, “partial” cross correlations so obtained can be normalized independently, usually  
 294 by whitening, before being summed.

295 We follow here the latter approach, but, instead of whitening, normalize by the power  
 296 spectral density  $\langle |s(\mathbf{x}, \omega)|^2 \rangle_{\mathbf{x}}$ , as in the left-hand side of eq. (30). As explained in sec. 2.3.2,  
 297  $\langle |s(\mathbf{x}, \omega)|^2 \rangle_{\mathbf{x}}$  is averaged over all stations  $\mathbf{x}$ , and is proportional, through eq. (29), to the  
 298 actual power spectral density  $|h(\omega)|^2$  of ambient noise. 6-hour long non-overlapping time  
 299 windows are normalized independently before being summed. We shall refer to this procedure  
 300 as PSD- (power spectral density) normalization. Examples of the factor  $\langle |s(\mathbf{x}, \omega)|^2 \rangle_{\mathbf{x}}$  are  
 301 shown in Fig. 3 for twenty different time windows, sampling all four seasons. The cumulative  
 302 power spectral density  $\langle |s(\mathbf{x}, \omega)|^2 \rangle_{\mathbf{x}}$  is shown in Fig. 4.

303 To verify that possible biases introduced by anomalous events are indeed suppressed by  
 304 PSD-normalization, we also attempted to remove them directly from the data. We define as  
 305 “event” the Fourier transform of one day of recording, and flag it as anomalous (an “outlier”)

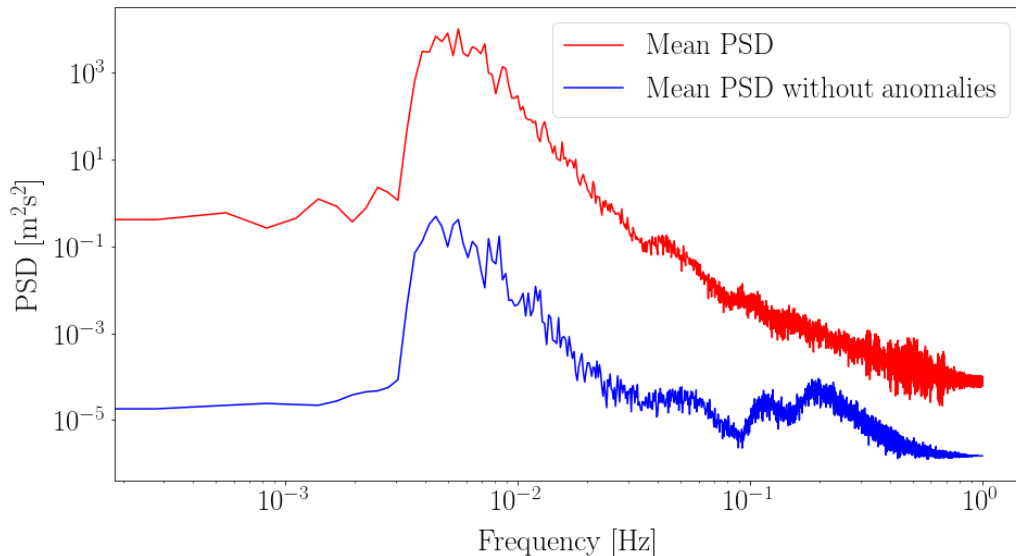


Figure 4: Power spectral density  $\langle |s(\mathbf{x}, \omega)|^2 \rangle_{\mathbf{x}}$  (red line) used to normalize the observed cross-spectra as in eq. (30). The power spectral density obtained after removing from the data all 24 hour-long time intervals where anomalous events (sec. 3.1) were recorded (blue line) is also shown.

306 if the maximum amplitude exceeds a certain value. After testing various criteria to identify  
 307 outliers, we decided to follow the Interquartile Range rule (IQR) [Tukey, 1977], with outlier  
 308 constant set to 5, which we applied separately on 2-month-long subsets of the entire data set.  
 309 The power spectral density  $\langle |s(\mathbf{x}, \omega)|^2 \rangle_{\mathbf{x}}$  obtained after removing the so defined outliers  
 310 is also shown in Fig. 4 for the sake of comparison. We show in Fig. 5 the cross correlation  
 311 of signals recorded over more than one year at several stations, before and after removing  
 312 outliers, as described. After conducting the same test on several other station pairs, we  
 313 conclude that the two approaches result in practically coincident results. We prefer PSD-  
 314 normalization as it involves no arbitrary choices, e.g. in the definition of outlier. In Fig. 6  
 315 the results of PSD-normalizing and whitening the same cross correlations are compared.  
 316 Discrepancies are, again, very small, which confirms the stability of our results.

317 Figs. 5 and 6 also show that the imaginary parts of our observed cross correlations can  
 318 be relatively large. This is in contrast with eq. (30), stipulating that the imaginary part  
 319 of the frequency-domain cross correlation should be zero (or, equivalently, the causal and  
 320 anticausal parts of the time-domain cross correlation should coincide [e.g. App. B of *Boschi*  
 321 *and Weemstra*, 2015]). The same limitation affects many other seismic ambient-noise studies,  
 322 where the conditions that the field be diffuse and that sources be uniformly distributed over  
 323 space are not exactly met. To quantify the azimuthal bias of recorded ambient signal, we  
 324 narrow-band-pass filter and inverse-Fourier-transform the frequency-domain cross-correlation  
 325 associated with each station pair; we then compute, in the time domain, the signal-to-noise  
 326 ratio (SNR) of both causal and anticausal parts of each cross correlation, defined as the  
 327 ratio of the maximum signal amplitude to the maximum of the trailing noise [e.g. *Yang*  
 328 *and Ritzwoller*, 2008; *Kästle et al.*, 2016]. The results are shown in Fig. 7, where it is  
 329 apparent that, because our array is small, its azimuthal sampling is limited (sampling is  
 330 particularly poor around the East-West direction). The sampled azimuths appear however

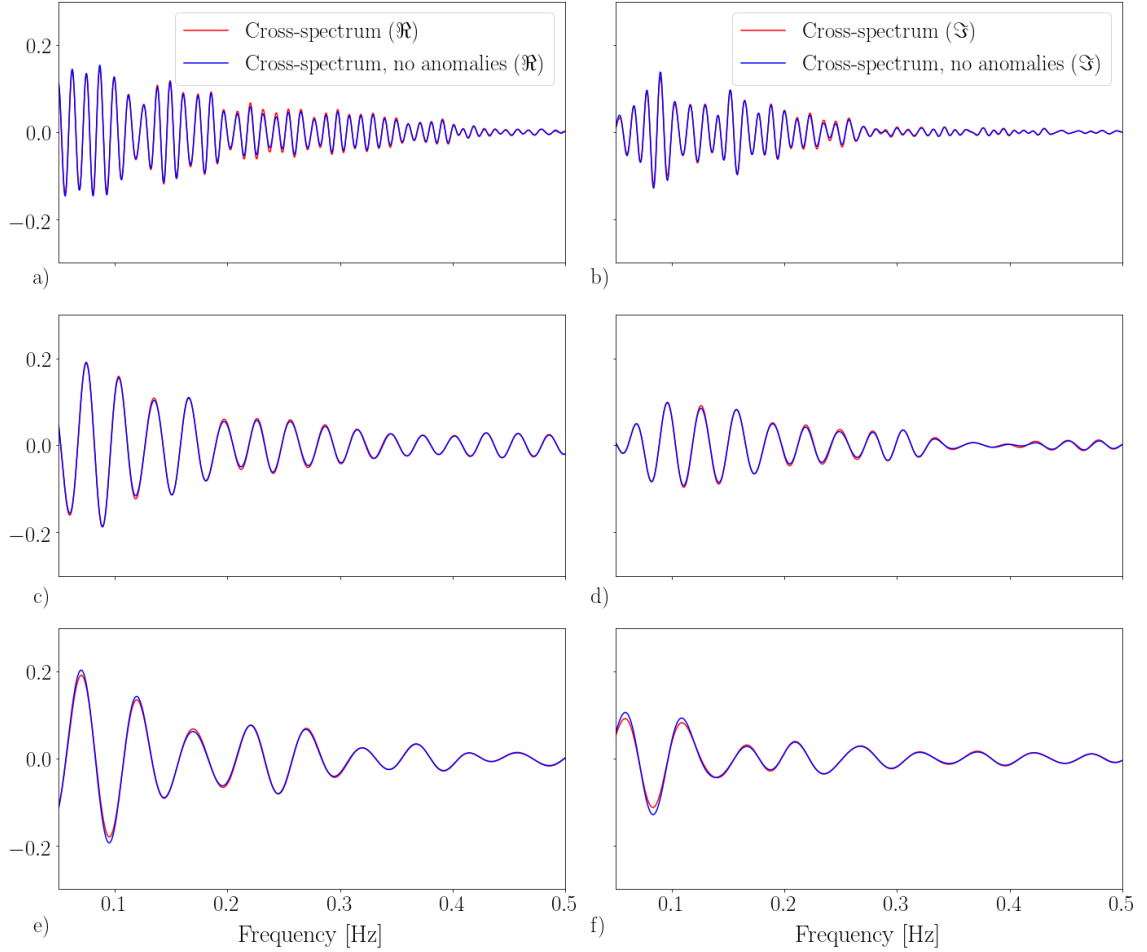


Figure 5: Real (a, c, e) and imaginary (b, d, f) parts of the cross correlations of the entire available recordings at stations UT.006 and UT.009 (a, b), IV.AGLI and IV.DGI (c, d), UT.002 and UT.003 (e, f). The associated interstation distances are 231, 97 and 57 km, respectively. Cross correlations of the entire recorded traces are PSD-normalized (red lines); alternatively (blue), outliers are removed from the traces prior to cross-correlating, as discussed in sec. 3.1. PSD-normalization is preferred throughout the rest of this study.

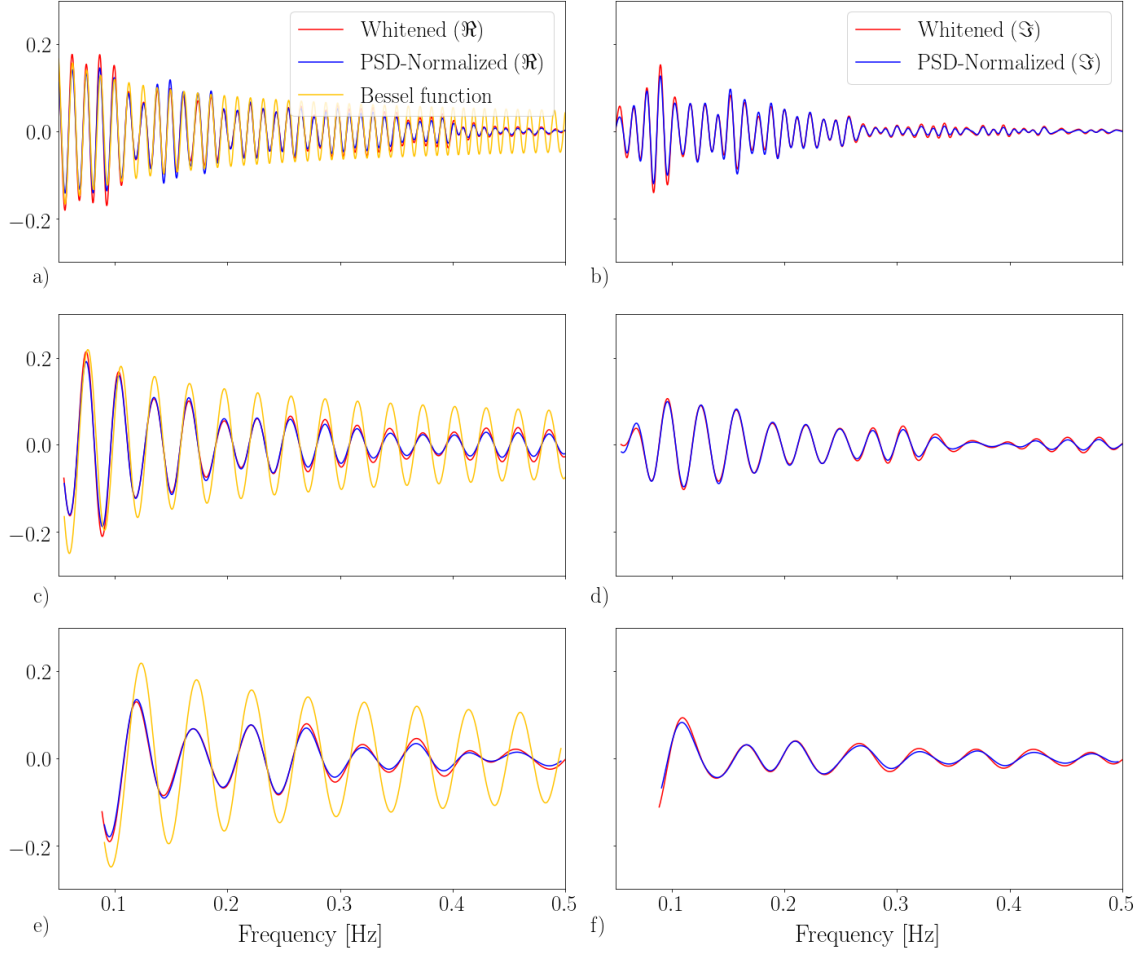


Figure 6: Same as Fig. 5, but PSD-normalized (red lines) and whitened cross correlations (blue) are now compared. In both cases, the entire available seismic records are cross correlated, without attempting to identify and remove outliers. For each interstation distance  $\Delta$ , the Bessel function  $J_0(\omega\Delta/c)$  (yellow), to which the real parts of cross correlations should be proportional according to (30), is also shown.

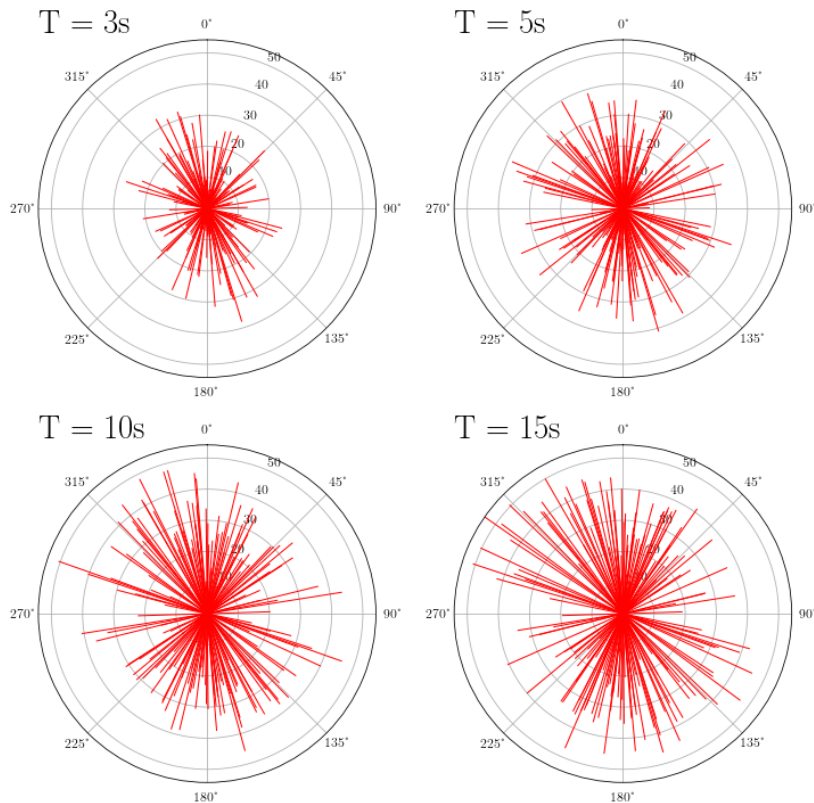


Figure 7: Estimates of the SNR of our cross correlations, as a function of station-pair azimuth, at periods of 3 to 15s, as specified. The value of SNR determines the length of the red segments, while their orientation coincides with the station-pair azimuth, with  $0^\circ$  corresponding to the North,  $90^\circ$  to the East, etc. The signal-to-noise ratios associated with both the causal and anticausal parts of the cross correlations are computed and plotted; for each station pair, the causal and anticausal segments point in opposite directions. In practice, longer segments should point to the direction where most seismic ambient signal comes from.

331 to be characterized, on average, by similar values of SNR, at least at periods  $\geq 5$ s, indicating  
 332 a relatively isotropic ambient field: compare, e.g., with Fig. 12 of *Kästle et al.* [2016], which  
 333 was obtained by applying the exact same procedure to a larger and denser array.

334 In the following, we shall further reduce the unwanted effects of azimuthal bias, by implicitly  
 335 averaging over all station pairs (and therefore all available azimuths) as only one model  
 336 of  $\alpha$  is sought that fits cross correlation data for all station pairs. Authors that process data  
 337 from larger/denser arrays often also group station pairs in distance bins, and for each distance  
 338 bin take an average over all azimuths [e.g. *Prieto et al.*, 2009; *Weemstra et al.*, 2013], but  
 339 this is not feasible in our case owing to the limited size of our array.

### 340 3.2 Dispersion and attenuation parameters

341 For each station pair  $i, j$ , a dispersion curve  $c_{ij}=c_{ij}(\omega)$  is derived via the frequency-domain  
 342 method of *Ekström et al.* [2009], *Boschi et al.* [2013], *Kästle et al.* [2016]. Specifically, the  
 343 algorithm of *Kästle et al.* [2016] is slightly modified, i.e. the data are PSD-normalized rather  
 344 than whitened; examples of dispersion curves resulting from both PSD-normalization and  
 345 whitening are shown in Fig. 8. After determining that both approaches lead to approx-  
 346 imately coincident results, we use in the following the dispersion curves obtained by PSD-

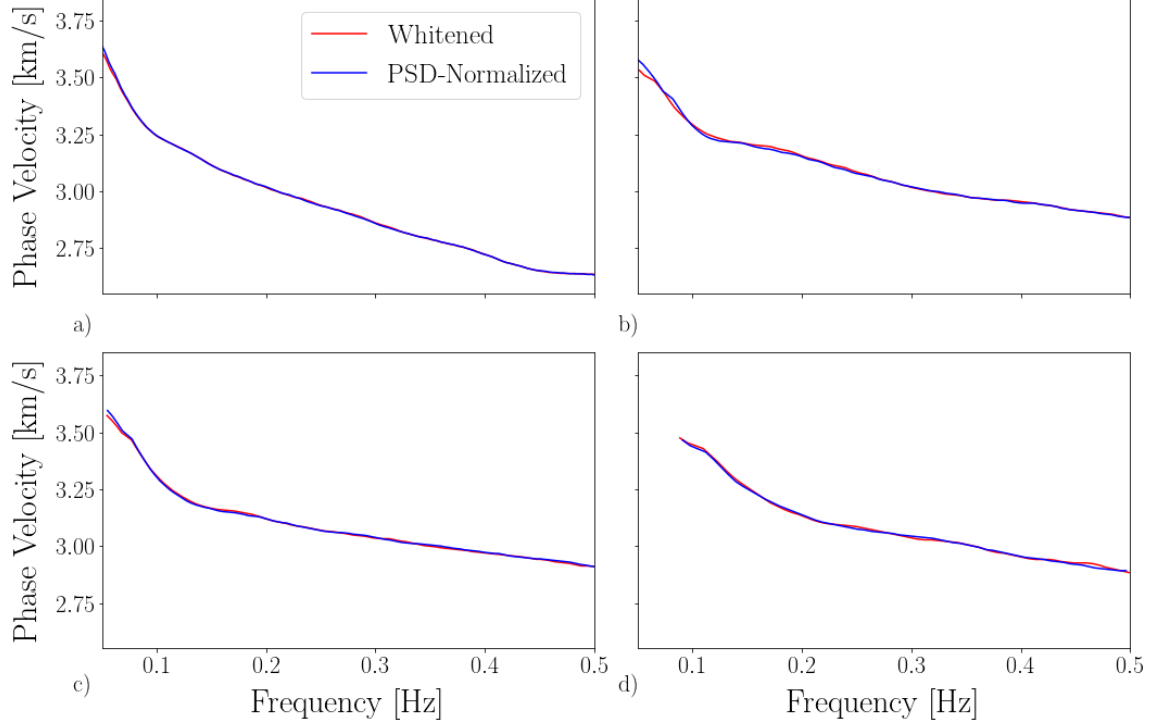


Figure 8: Phase velocity curves retrieved from the whitened (red lines) and PSD-normalized (blue) cross-spectra, for station pairs (a) UT.006 - UT.009 (interstation distance  $\sim 231$  km), (b) UT.002 - UT.004 ( $\sim 152$  km), (c) IV.AGLI - IV.DGI ( $\sim 97$  km), and (d) UT.002 - UT.003 ( $\sim 57$  km).

347 normalization. Importantly, in both cases the frequency range over which the dispersion curve  
 348 is defined changes depending on the station pair; as a general rule, it is hard to constrain its  
 349 low-frequency end if stations are relatively close to one another.

### 350 3.2.1 Attenuation parameter as a scalar constant

351 Taking the squared modulus of the difference of the left- and right-hand sides of eq. (30), and  
 352 summing over all frequency samples  $\omega_k$  and station pairs  $i, j$ , the cost function

$$\sum_{i,j} \sum_k \left| \frac{s(\mathbf{x}_i, \omega_k) s^*(\mathbf{x}_j, \omega_k)}{\langle |s(\mathbf{x}, \omega_k)|^2 \rangle_{\mathbf{x}}} - \frac{2c_{ij}(\omega_k)}{\omega_k \sqrt{2\pi}} \frac{1}{I[\alpha, \omega_k, c_{ij}(\omega_k)]} J_0 \left( \frac{\omega_k |\mathbf{x}_i - \mathbf{x}_j|}{c_{ij}(\omega_k)} \right) \frac{e^{-\alpha |\mathbf{x}_i - \mathbf{x}_j|}}{\alpha} \right|^2 \quad (33)$$

353 is obtained.

354 The right-hand side of eq. (30) is, through the Bessel function  $J_0$ , an oscillatory function  
 355 of  $\omega$ . The value of the attenuation parameter  $\alpha$ , however, only affects its envelope, and not  
 356 its oscillations, with respect to  $\omega$ . Following other authors who estimated attenuation on the  
 357 basis of ambient-noise cross correlation [e.g., Prieto *et al.*, 2009], we accordingly define the

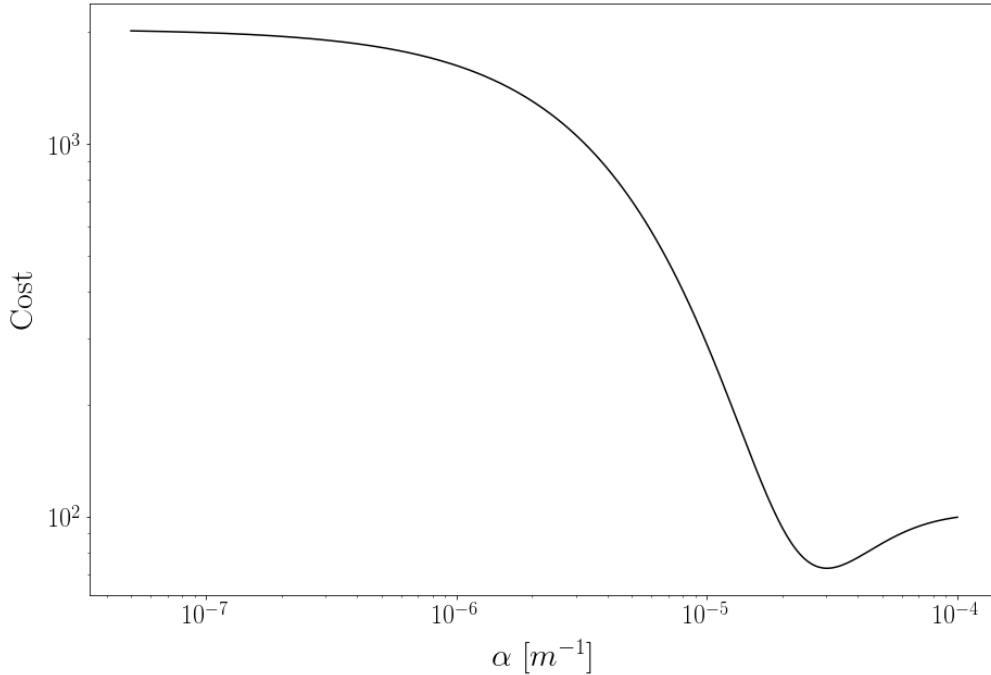


Figure 9: Cost  $C_1$  as defined by eq. (34), as a function of the scalar attenuation parameter  $\alpha$ .

358 cost function

$$\begin{aligned}
 C_1(\alpha) = & \sum_{i,j} \sum_k \left| \text{env} \left[ \frac{s(\mathbf{x}_i, \omega_k) s^*(\mathbf{x}_j, \omega_k)}{\langle |s(\mathbf{x}, \omega_k)|^2 \rangle_{\mathbf{x}}} \right] \right. \\
 & \left. - \text{env} \left[ \frac{2c_{ij}(\omega_k)}{\omega_k \sqrt{2\pi}} \frac{1}{I[\alpha, \omega_k, c_{ij}(\omega_k)]} J_0 \left( \frac{\omega_k |\mathbf{x}_i - \mathbf{x}_j|}{c_{ij}(\omega_k)} \right) \frac{e^{-\alpha |\mathbf{x}_i - \mathbf{x}_j|}}{\alpha} \right] \right|^2, \quad (34)
 \end{aligned}$$

359 where  $\text{env}$  denotes the envelope function, which we implement by fitting a linear combination  
 360 of splines [e.g. *Press et al.*, 1992] to the maxima of the absolute value of its argument.

361 The attenuation parameter  $\alpha$  in this case is a scalar value, independent of both frequency  
 362 and location. We show in Fig. 9 how  $C_1$  varies as a function of  $\alpha$ ; a clear minimum is identified  
 363 at  $\alpha = 3.03 \times 10^{-5} \text{ m}^{-1}$ , which is our preferred attenuation model in this scenario. We next  
 364 use this value for  $\alpha$  to evaluate numerically the right-hand side of eq. (30), and compare  
 365 the results with the normalized cross-correlation at the left-hand side; this is illustrated in  
 366 Fig. 10 for four different station pairs. The modeled Green's functions have their zeroes at  
 367 approximately the same frequencies as the measured ones, indicating that dispersion curves  
 368 derived as described above are reliable. At short interstation distances, the found value of  
 369  $\alpha$  also results in a relatively good fit of observed amplitude at most frequencies. The fit  
 370 deteriorates with increasing distance, indicating that the assumption that  $\alpha$  be constant does  
 371 not honour the actual complexity of the medium.

372 As an additional test, we found the cost function defined by expression (33) (i.e., no  
 373 envelopes are taken) to be similar to  $C_1$ , with a less prominent but well defined minimum at  
 374  $\alpha = 2.75 \times 10^{-5} \text{ m}^{-1}$ . The similarity of this estimate of  $\alpha$  with the one based on function  $C_1$

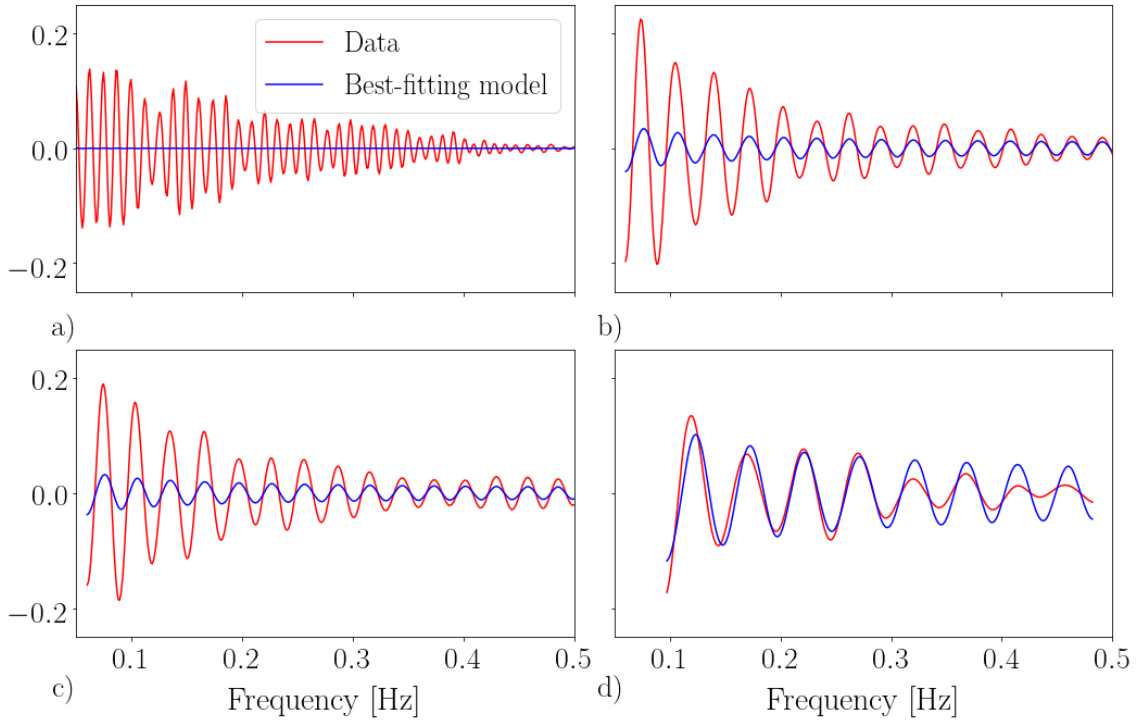


Figure 10: Comparison of normalized data (red lines) and model (blue), i.e. left- and right-hand side of eq. (30), after substituting  $\alpha=3.03 \times 10^{-5} \text{ m}^{-1}$ , as explained in sec. 3.2.1 (i.e., inversion via the cost function  $C_1$ ). As in Fig. 8, panels a, b, c and d correspond to station pairs UT.006-UT.009, UT.002 - UT.004, IV.AGLI-IV.DGI and UT.002-UT.003, respectively, with interstation distances decreasing from 231 to 57 km.

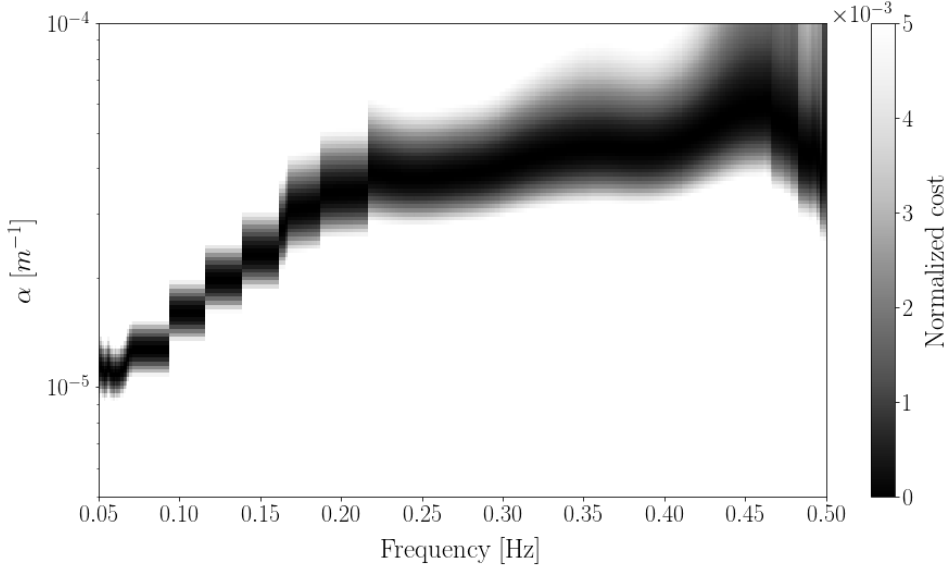


Figure 11: Cost function  $C_2(\alpha, \omega)$  (sec. 3.2.2) shown (after normalization) as a function of the attenuation parameter  $\alpha$  and frequency  $\omega$ . We normalize  $C_2$  according to the formula  $\frac{C_2(\alpha, \omega) - \min[C_2(\alpha, \omega)]}{\max[C_2(\alpha, \omega)] - \min[C_2(\alpha, \omega)]}$ , where  $\min[C_2]$  and  $\max[C_2]$  denote the minimum and maximum values of  $C_2$  for all sampled values of  $\alpha$  and  $\omega$ . The stepwise trend of the minima of  $C_2$  is correlated with the stepwise growth (also as a function of  $\omega$ ) of the number of station pairs for which cross-correlation data are available.

375 suggests that this result is robust.

### 376 3.2.2 Frequency-dependent attenuation parameter

377 We next allow the attenuation parameter  $\alpha$  to change as a function of  $\omega$ ; in practice, we  
378 evaluate the cost function

$$\begin{aligned}
 C_2(\alpha, \omega) = \sum_{i,j} & \left| \text{env} \left[ \frac{s(\mathbf{x}_i, \omega) s^*(\mathbf{x}_j, \omega)}{\langle |s(\mathbf{x}, \omega)|^2 \rangle_{\mathbf{x}}} \right] \right. \\
 & \left. - \text{env} \left[ \frac{2c_{ij}(\omega)}{\omega\sqrt{2\pi}} \frac{1}{I[\alpha(\omega), \omega, c_{ij}(\omega)]} J_0 \left( \frac{\omega|\mathbf{x}_i - \mathbf{x}_j|}{c_{ij}(\omega)} \right) \frac{e^{-\alpha|\mathbf{x}_i - \mathbf{x}_j|}}{\alpha} \right] \right|^2, \quad (35)
 \end{aligned}$$

379 shown in Fig. 11, after normalization, as a function of both  $\alpha$  and  $\omega$ . Since both terms within  
380 the square brackets in eq. (35) are close to a Bessel function of  $\omega$ , it is not surprising that  
381 their difference has an oscillatory behaviour with respect to  $\omega$ ; because only a discrete and  
382 limited set of interstation distances are available from our data set, this effect is not canceled  
383 by summation, as is apparent from Fig. 11. Fig. 11 also shows that  $C_2(\alpha, \omega)$  has a single,  
384 well-defined minimum at all frequencies, resulting in the  $\alpha(\omega)$  curve of Fig. 12.

385 The actual values of the minima of  $C_2(\alpha, \omega)$ , without normalization, are shown in Fig. 12.  
386  $C_2$  decreases with growing  $\omega$ , meaning that relatively high frequencies are better fit than low  
387 frequencies. Fig. 13 also shows that the amplitude fit between observed cross correlations  
388 and modeled Green's functions is worse for large interstation distances.

389 In analogy with sec. 3.2.1, we also evaluated an alternative cost function, where the differ-  
390 ence of observed and theoretical, normalized cross correlation is computed without extracting

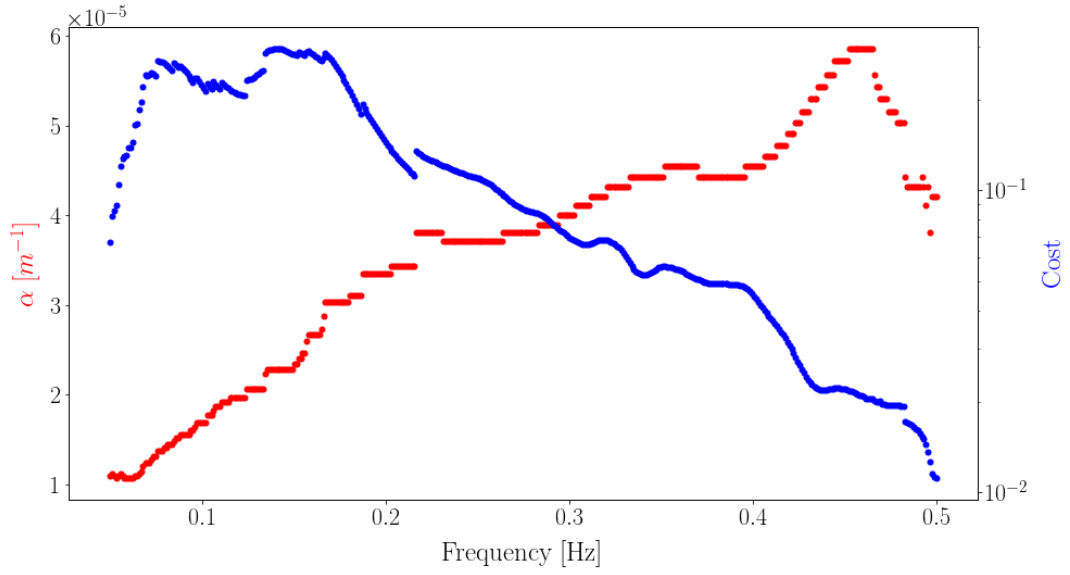


Figure 12: Attenuation parameter  $\alpha$  (red dots, scale on the left) and corresponding values of the cost function  $C_2(\alpha, \omega)$  (blue dots, scale on the right), both plotted as functions of frequency  $\omega$ .

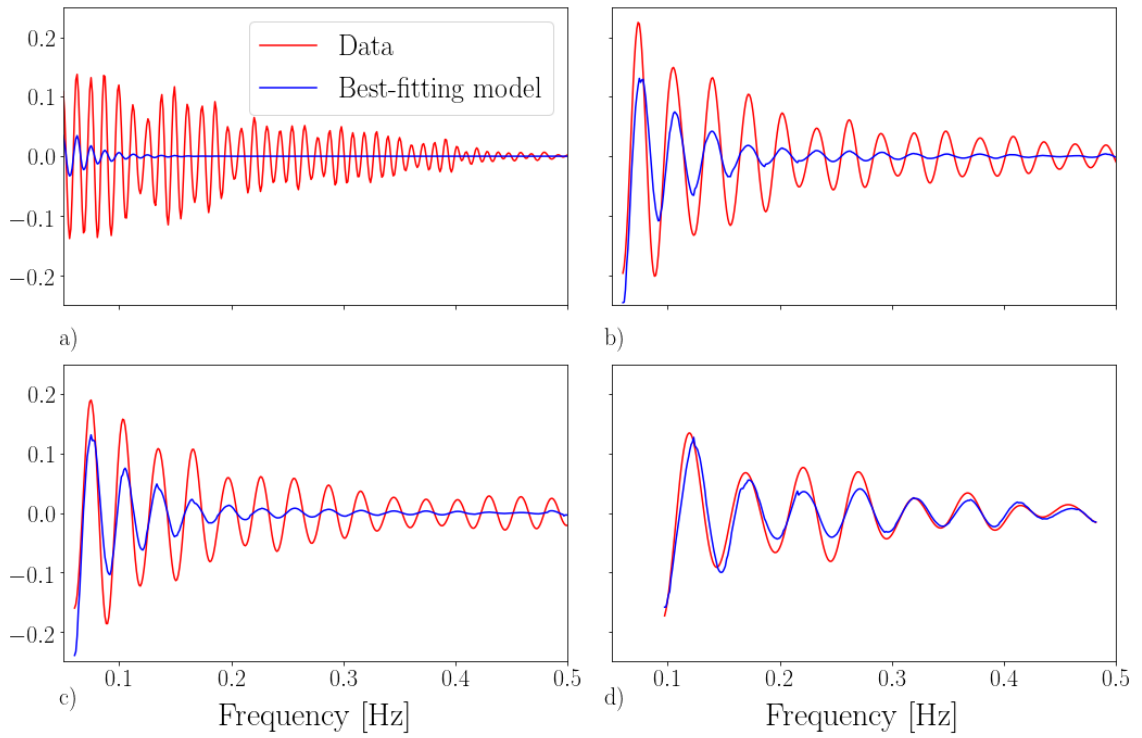


Figure 13: Same as Fig. 10, but the blue curves are obtained by substituting into eq. (30) the values of  $\alpha(\omega)$  obtained by minimizing the cost function  $C_2$  of sec. 3.2.2.

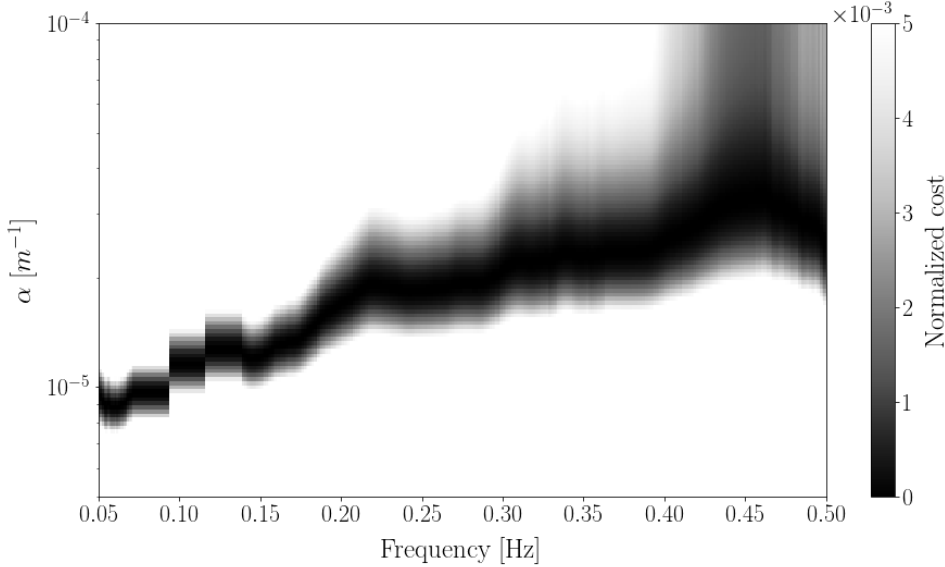


Figure 14: Same as Fig. 11, but the cost function  $C_3$  is evaluated, where contributions of different station pairs are weighted differently (sec. 3.2.3) according to interstation distance.

391 their envelopes. This function varies more rapidly than  $C_2$  does, with respect to both  $\alpha$  and  
 392  $\omega$ ; but it spans a similar range of values and, like  $C_2$ , has a unique minimum at all frequencies.  
 393 The corresponding values of  $\alpha$  are similar to those obtained based on  $C_2$ ; we do not show or  
 394 discuss them here in the interest of brevity.

### 395 3.2.3 Cost function as a weighted sum

396 Attenuation models of secs. 3.2.1 and 3.2.2 achieve a systematically worse fit of cross corre-  
 397 lations between faraway as opposed to nearby stations (see examples in Figs. 10 and 13).  
 398 To some (minor) extent, this bias might stem from the error involved in the far-field/high-  
 399 frequency approximation discussed in sec. 2.1, causing a fictitious loss of amplitude of the  
 400 theoretical cross correlation at large interstation distances (Fig. 1). More importantly, it  
 401 might result from the fact that, by geometrical spreading, cross-correlation amplitude de-  
 402 creases with growing interstation distance; assuming the *relative* misfit on cross-correlation  
 403 amplitude to be independent of distance, pairs of faraway stations are then systematically  
 404 associated with smaller *absolute* errors and thus contribute less to the cost functions  $C_1$  and  
 405  $C_2$ . We attempt to reduce this effect by replacing the sum in  $C_2$  with a weighted sum,

$$\begin{aligned}
 C_3(\alpha, \omega) = & \sum_{i,j} w(|\mathbf{x}_i - \mathbf{x}_j|) \left| \text{env} \left[ \frac{s(\mathbf{x}_i, \omega) s^*(\mathbf{x}_j, \omega)}{\langle |s(\mathbf{x}, \omega)|^2 \rangle_{\mathbf{x}}} \right] \right. \\
 & \left. - \text{env} \left[ \frac{2c_{ij}(\omega)}{\omega \sqrt{2\pi}} \frac{1}{I[\alpha(\omega), \omega, c_{ij}(\omega)]} J_0 \left( \frac{\omega |\mathbf{x}_i - \mathbf{x}_j|}{c_{ij}(\omega)} \right) \frac{e^{-\alpha |\mathbf{x}_i - \mathbf{x}_j|}}{\alpha} \right] \right|^2, \quad (36)
 \end{aligned}$$

406 where  $w(|\mathbf{x}_i - \mathbf{x}_j|) = |\mathbf{x}_i - \mathbf{x}_j|^e$  and  $e$  is the Euler number. We selected this weighting  
 407 scheme after a suite of preliminary tests, where the weight  $w$  was chosen to coincide in turn  
 408 with different powers (from square root to fourth power) of interstation distance. We show  
 409  $C_3(\alpha, \omega)$  in Fig. 14, and the corresponding best-fitting values of  $\alpha$  in Fig. 15. Interestingly,

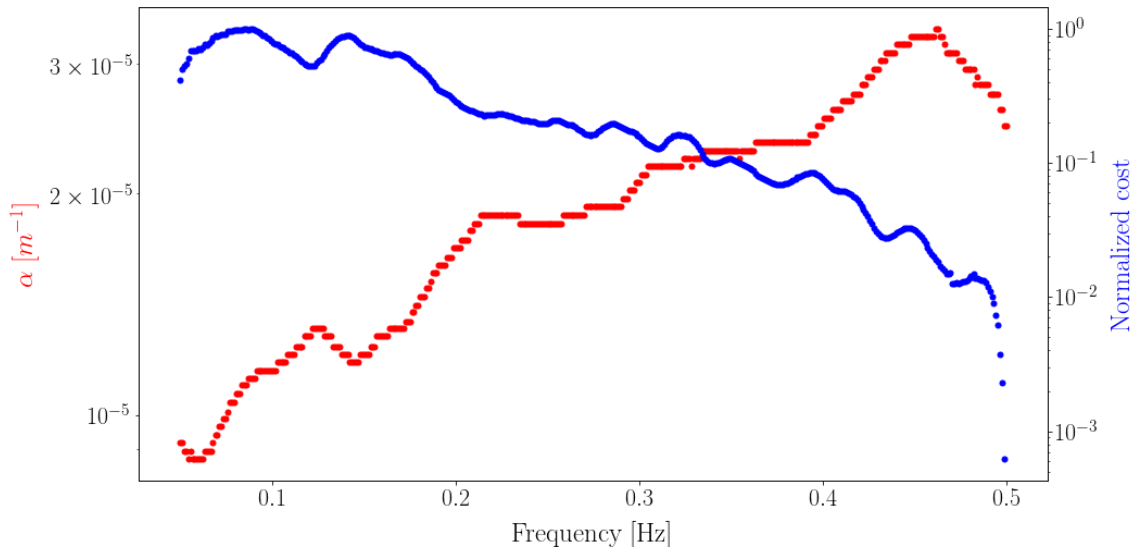


Figure 15: Same as Fig. 12, but the values  $\alpha(\omega)$  (red dots) that minimize at each  $\omega$  the cost function  $C_3$  (sec. 3.2.3), and the corresponding values of  $C_3$  (blue dots) are shown.

410 it is apparent from Fig. 15 that the so obtained function  $\alpha(\omega)$  spans a smaller range of values  
 411 than its counterpart discussed in sec. 3.2.2;  $\alpha$  is also generally smaller, resulting in larger  
 412 amplitude of modeled cross correlations (Fig. 16) at all interstation distances.

413 We are unable to determine a unique function  $\alpha(\omega)$  that results in a comparably good fit of  
 414 cross-correlation amplitude for all station pairs: observed amplitudes tend to be overestimated  
 415 by our “model” at short interstation distances, and underestimated at large interstation  
 416 distances. This effect might point to possible lateral heterogeneities of  $\alpha$  that our data set  
 417 is too limited to constrain; it could also be associated with the error inherent in ambient-  
 418 noise-based reconstruction of the Green’s function, when the seismic ambient field (as in most  
 419 practical applications) is not truly diffuse.

## 420 4 Discussion and conclusions

421 The main purpose of this study was to clarify some aspects of the relationship between the  
 422 cross correlation of seismic ambient noise and surface-wave attenuation (attenuation param-  
 423 eter  $\alpha$  or quality factor  $Q$ ). It is known that this relationship is complicated by the need  
 424 to process ambient-noise cross correlation data so as to reduce as much as possible the bias  
 425 introduced by anomalous high-amplitude events (earthquakes). This is often achieved by  
 426 subdividing continuous traces into shorter time intervals, which are then whitened and cross-  
 427 correlated separately before being “stacked” together; but whitening has a complicated effect  
 428 on the mentioned noise-attenuation relationship [Weemstra *et al.*, 2014]. We develop here a  
 429 different normalization criterion, with practical effects similar to whitening, but obtained by  
 430 simply manipulating the reciprocity theorem without any additional data processing. This  
 431 results in the relationship (30), which is strictly valid provided that sources of seismic ambient  
 432 noise be uniformly distributed over  $\mathbb{R}^2$ , that their phases be random and uncorrelated, and  
 433 that the spectrum of noise sources be spatially uniform (sec. 2.3.2). Our experimental setup,

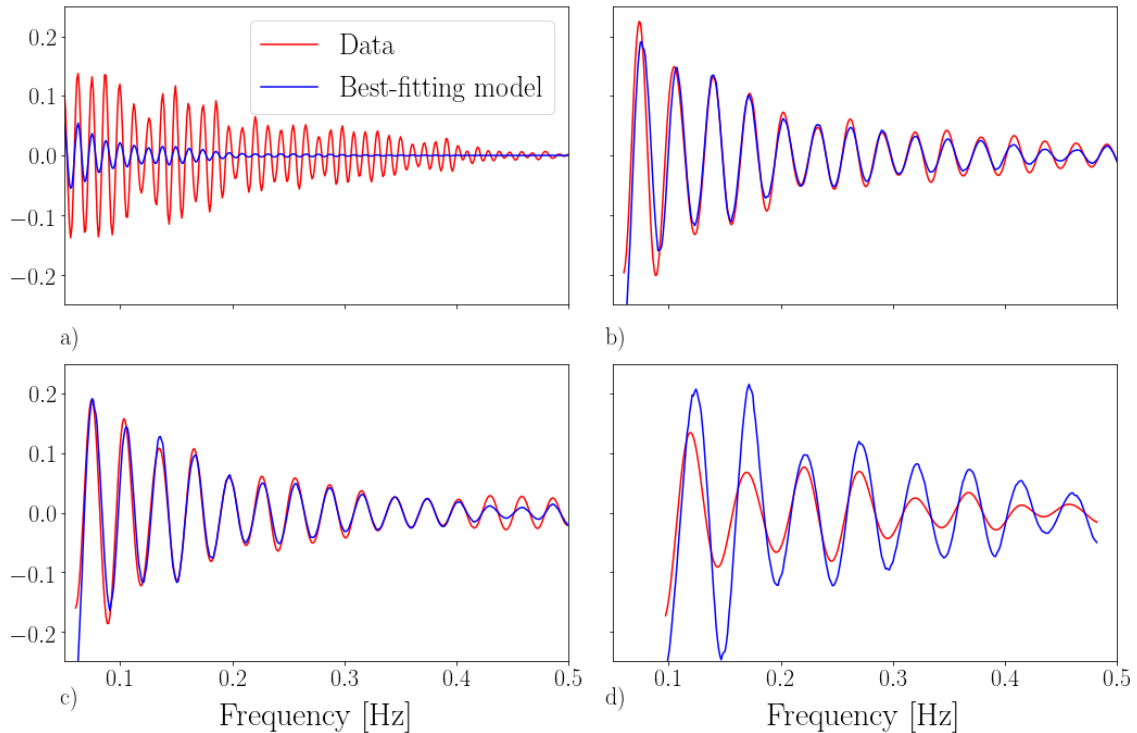


Figure 16: Same as Figs. 10 and 13, but the blue curves are obtained by substituting into eq. (30) the values of  $\alpha(\omega)$  obtained by minimizing the cost function  $C_3$  (sec. 3.2.3).

434 consisting of a small array deployed on an island, is chosen to approximately satisfy these  
 435 requirements.

436 Eq. (30) involves a proportionality factor, relating normalized cross-correlation and the  
 437 product  $J_0(\omega\Delta/c)e^{-\alpha\Delta}$  (with  $\Delta$  denoting interstation distance), that had been neglected in  
 438 previous studies. Compare, e.g., with eq. (7) of *Prieto et al.* [2009] or eq. (1) of *Lawrence and*  
 439 *Prieto* [2011]. The need to account for such a factor was pointed out theoretically by *Tsai*  
 440 [2011], while *Harmon et al.* [2010] and *Weemstra et al.* [2013] introduced it as a free parameter  
 441 of their inversions. Similar to *Tsai* [2011], we have derived an analytical expression for it,  
 442 and evaluate it numerically based on our estimates for  $\alpha$  and phase velocity  $c(\omega)$ . Fig. 17  
 443 shows that the factor in question is of the order of unity, which would explain the success of  
 444 *Prieto et al.* [2009], *Lawrence and Prieto* [2011] and others in inferring reasonable values for  
 445  $\alpha$ .

446 On the basis of eq. (30), we explored several possible definitions of cost function (secs.  
 447 3.2.1 through 3.2.3), quantifying the misfit between observed and modeled cross-correlation  
 448 amplitudes. We first assumed the attenuation parameter  $\alpha$  to be constant, independent of  
 449 frequency and position. We next identified a frequency-dependent  $\alpha = \alpha(\omega)$  model that  
 450 minimizes the misfit for all receiver-receiver pairs at the same time. Since the cost function  
 451 involves a sum over station pairs, we finally introduced a cost function where the contribution  
 452 of each station pair was weighted differently depending on interstation distance.

453 To compare quantitatively the misfit achieved by different models, let us introduce the

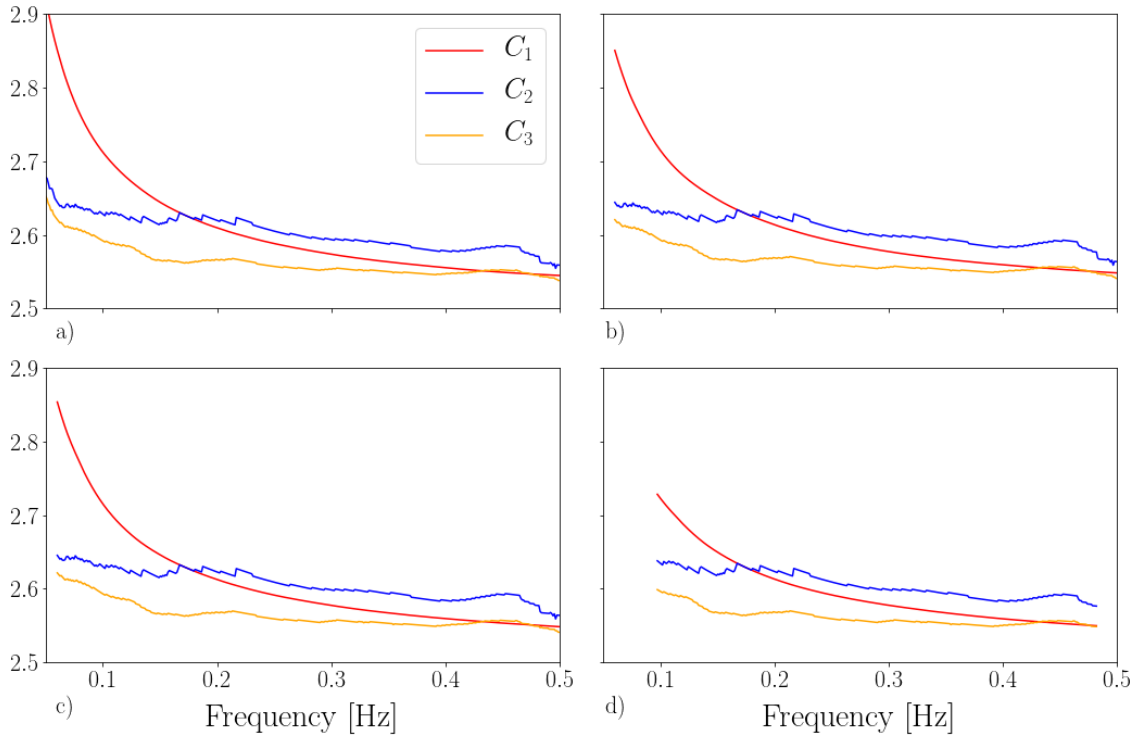


Figure 17: Proportionality factor  $\sqrt{\frac{2}{\pi}}c/[\alpha\omega I(\alpha,\omega,c)]$  relating normalized cross correlation and  $J_0(\omega\Delta/c)e^{-\alpha\Delta}$  in eq. (30). Its numerical value is evaluated based on inferred dispersion curves  $c(\omega)$ , and estimates for  $\alpha$  obtained by minimization of the cost functions  $C_1, C_2, C_3$  (each denoted by a different color, as specified). Panels (a) through (d) correspond to the same station pairs used as examples in previous figures.

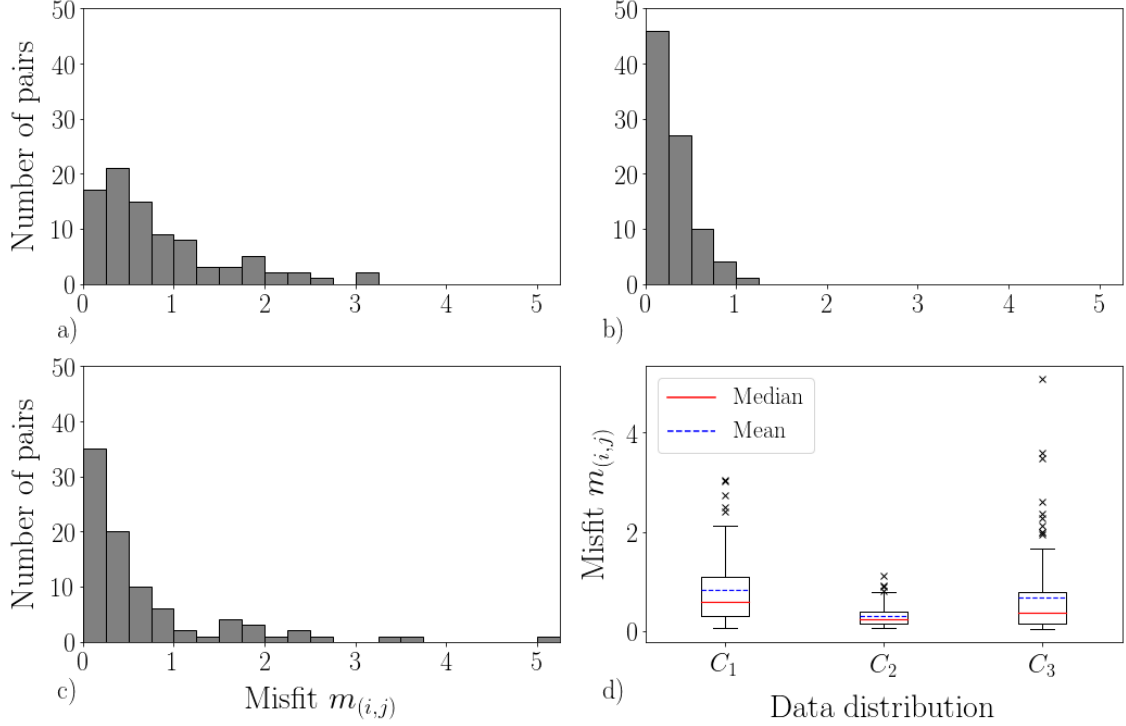


Figure 18: Number (vertical axis) of station pairs for which the misfit  $m_{ij}$  falls within a given interval (horizontal axis), for models of  $\alpha$  resulting from the minimization of cost functions (a)  $C_1$ , (b)  $C_2$ , and (c)  $C_3$ . (d) Box plots [Tukey, 1977] of the distributions at (a), (b) and (c).

454 misfit function

$$\begin{aligned}
 m_{ij} = \sum_k \left| \frac{s(\mathbf{x}_i, \omega_k) s^*(\mathbf{x}_j, \omega_k)}{\langle |s(\mathbf{x}, \omega_k)|^2 \rangle_{\mathbf{x}}} \right. \\
 \left. - \frac{2c_{ij}(\omega_k)}{\omega_k \sqrt{2\pi}} \frac{1}{I[\alpha(\omega_k), \omega_k, c_{ij}(\omega_k)]} J_0 \left( \frac{\omega_k |\mathbf{x}_i - \mathbf{x}_j|}{c_{ij}(\omega_k)} \right) \frac{e^{-\alpha(\omega_k) |\mathbf{x}_i - \mathbf{x}_j|}}{\alpha(\omega_k)} \right|^2, \quad (37)
 \end{aligned}$$

455 associated to the station pair  $ij$ . We implement eq. (37) for each model (corresponding to  
 456 the cost functions  $C_1$  through  $C_3$ ) and for each station pair  $ij$ , and visualize the resulting  
 457 values of  $m_{ij}$  in Fig. 18, in the form of one histogram per model.

458 It is apparent from Fig. 18, and could be anticipated from a visual comparison of Fig. 10  
 459 with Fig. 13, that allowing  $\alpha$  to vary with respect to  $\omega$  results in an overall improvement of  
 460 fit with respect to constant- $\alpha$  models. Minimizing the cost function  $C_3$ , on the other hand,  
 461 results in an increase in the misfit  $m_{ij}$  with respect to  $C_2$ , as nearby station pairs tend to  
 462 contribute to  $m_{ij}$  more than faraway ones (see discussion of the cost function  $C_2$  in sec.  
 463 3.2.3). We found by a Kolmogorov-Smirnoff test [e.g. Press et al., 1992] that the probability  
 464 that the three histograms in Fig. 18 correspond to the same statistical distribution is always  
 465  $\lesssim 3\%$ , and always  $\lesssim 1\%$  for the histogram in Fig. 18b ( $C_2$  in Fig. 18d). This suggests that the  
 466 improvement in fit achieved by the cost function  $C_2$  is significant. Only a limited number of  
 467 samples (station pairs) is available, however, and a more reliable statistical analysis should  
 468 be conducted in the future on a larger database. In addition, the level of complexity (number

469 of degrees of freedom) in the function  $\alpha=\alpha(\omega)$  that can be constrained by the available data  
470 remains to be determined; it is beyond the scope of our current contribution.

471 It would be useful to compare our observations with independent estimates of  $\alpha$  in the  
472 region of interest, but, to our knowledge, no studies of surface-wave attenuation in Sardinia  
473 have been published so far. Comparison with global surface-wave attenuation literature  
474 suggests that our estimates of  $\alpha$  (on the order of  $10^{-5}\text{m}^{-1}$  in the period range 2-10s according  
475 to Figs. 12 and 15) are relatively large. Studies based on earthquake data suggest values of  
476  $\alpha$  on the order of  $10^{-6}\text{m}^{-1}$ , but quickly growing, with decreasing period, within the period  
477 range of interest to us [Mitchell, 1995; Romanowicz and Mitchell, 2015]. Surface waves at  
478 those periods are perhaps best sampled by ambient-noise cross correlations; Prieto *et al.*  
479 [2009] find  $\alpha\approx 6.4 \times 10^{-6}\text{m}^{-1}$  from seismic ambient noise at 5s period, consistent with the  
480 laterally-varying values obtained by Lawrence and Prieto [2011], and not far from the values  
481 proposed here; Lin *et al.* [2011] estimate  $\alpha\approx 1 \times 10^{-6}\text{m}^{-1}$  or lower. Those studies neglect the  
482 proportionality factor shown here in Fig. 17, which might partially explain the discrepancy.  
483 Both Harmon *et al.* [2010] and Weemstra *et al.* [2013] account for this effect, although in a  
484 different way than done here; Harmon *et al.* [2010] find  $\alpha\approx 5 \times 10^{-7}\text{m}^{-1}$  at 7.5s period, while  
485 Weemstra *et al.* [2013] obtain estimates of  $\alpha$  actually *larger* than ours. Viens *et al.* [2017]  
486 likewise fit ambient-noise surface-wave data with  $\alpha=1.4 \times 10^{-5}\text{m}^{-1}$  in the period range 3-10s,  
487 consistent with our estimates.

488 As values of  $\alpha$  obtained from different methods are compared, one should keep in mind the  
489 significant uncertainties associated with the many practical issues quantified, e.g., by Menon  
490 *et al.* [2014]. Estimates of surface-wave attenuation might be affected by the presence, in  
491 seismic ambient noise, of body-wave signal not accounted for by the theory [e.g. Gerstoft  
492 *et al.*, 2008]. Differences in the terrains where the data were collected also play a role.

493 This preliminary application, limited to a small data set, demonstrates that our new  
494 algorithm leads to reasonable estimates of  $\alpha$ . Future applications to denser instrument arrays,  
495 with a more thorough account of heterogeneity in source distribution, are likely to benefit  
496 more significantly from the theoretical improvements that we have introduced.

## 497 Acknowledgments

498 Our many exchanges with Julien de Rosny, Emanuel Kaestle, Piero Poli, Victor Tsai and  
499 Kees Weemstra were very beneficial to this study. We are also grateful to Nicholas Harmon,  
500 one anonymous reviewer and the editor Ana Ferreira for carefully reading and commenting  
501 our manuscript.

## 502 References

503 Abramowitz, M., and I. A. Stegun, *Handbook of Mathematical Functions*, National Bureau  
504 of Standards–Applied Mathematics Series, 1964.

505 Arduin, F., E. Stutzmann, M. Schimmel, and A. Mangeney, Modelling secondary  
506 microseismic noise by normal mode summation, *J. Geophys. Res.*, 116, C09,004,  
507 doi:10.1029/2011JC006,952, 2011.

- 508 Bensen, G. D., M. H. Ritzwoller, M. P. Barmin, A. L. Levshin, F. Lin, M. P. Moschetti,  
509 N. M. Shapiro, and Y. Yang, Processing seismic ambient noise data to obtain reliable  
510 broad-band surface wave dispersion measurements, *Geophys. J. Int.*, *169*(3), 1239–1260,  
511 DOI:10.1111/j.1365–246X.2007.03,374.x, 2007.
- 512 Boschi, L., and C. Weemstra, Stationary-phase integrals in the cross-correlation of ambient  
513 noise, *Rev. Geophys.*, *53*, doi:10.1002/2014RG000,455, 2015.
- 514 Boschi, L., C. Weemstra, J. Verbeke, G. Ekström, A. Zunino, and D. Giardini, On measur-  
515 ing surface wave phase velocity from station-station cross-correlation of ambient signal,  
516 *Geophys. J. Int.*, *192*(1), 346–358,doi:10.1093/gji/ggs023, 2013.
- 517 Boschi, L., I. Molinari, and M. Reinwald, A simple method for earthquake location by surface-  
518 wave time-reversal, *Geophys. J. Int.*, *215*, 1–21, 2018.
- 519 Campillo, M., and P. Roux, Seismic imaging and monitoring with ambient noise correlations,  
520 in *Treatise of Geophysics. Vol. 1*, edited by B. Romanowicz and A. M. Dziewonski, Elsevier,  
521 2014.
- 522 Cupillard, P., and Y. Capdeville, On the amplitude of surface waves obtained by noise cor-  
523 relation and the capability to recover the attenuation: a numerical approach, *Geophys. J.*  
524 *Int.*, *181*(3), 1687–1700, doi:10.1111/j.1365–246X.2010.04,586.x, 2010.
- 525 DLMF, *NIST Digital Library of Mathematical Functions*, <http://dlmf.nist.gov/>, Release  
526 1.0.20 of 2018-09-15, f. W. J. Olver, A. B. Olde Daalhuis, D. W. Lozier, B. I. Schnei-  
527 der, R. F. Boisvert, C. W. Clark, B. R. Miller and B. V. Saunders, eds.
- 528 Ekström, G., G. A. Abers, and S. C. Webb, Determination of surface-wave phase veloci-  
529 ties across USArray from noise and Aki’s spectral formulation, *Geophys. Res. Lett.*, *36*,  
530 doi:10.1029/2009GL039,131, 2009.
- 531 Gerstoft, P., P. M. Shearer, N. Harmon, and J. Zhang, Global P, PP, and PKP wave micro-  
532 seisms observed from distant storms, *Geophys. Res. Lett.*, *35*, doi:10.1029/2008GL036,111,  
533 2008.
- 534 Harmon, N., C. Rychert, and P. Gerstoft, Distribution of noise sources for seismic interfer-  
535 ometry, *Geophys. J. Int.*, *183*, 1470–1484, doi:10.1111/j.1365–246X.2010.04,802.x, 2010.
- 536 Hildebrand, F. B., *Advanced Calculus for Applications (second edition)*, Prentice-Hall, En-  
537 glewood Cliffs, N. J., 1976.
- 538 Hillers, G., N. Graham, M. Campillo, S. Kedar, M. Landes, and N. Shapiro, Global oceanic  
539 microseism sources as seen by seismic arrays and predicted by wave action models,  
540 *Geochem. Geophys. Geosyst.*, *13*, Q01,021, doi:10.1029/2011GC003,875, 2012.
- 541 Kästle, E., R. Soomro, C. Weemstra, L. Boschi, and T. Meier, Two-receiver measurements  
542 of phase velocity: cross-validation of ambient-noise and earthquake-based observations,  
543 *Geophys. J. Int.*, *207*, 1493–1512, 2016.
- 544 Kinsler, L. E., A. R. Frey, A. B. Coppens, and J. V. Sanders, *Fundamentals of Acoustics*  
545 *(fourth edition)*, Wiley & Sons, Hoboken, N. J., 1999.

- 546 Lawrence, J. F., and G. A. Prieto, Attenuation tomography of the western United States  
547 from ambient seismic noise, *J. Geophys. Res.*, *116*, 2011.
- 548 Lin, F.-C., M. H. Ritzwoller, and W. Shen, On the reliability of attenuation measurements  
549 from ambient noise cross-correlations, *Geophys. Res. Lett.*, *38*, 2011.
- 550 Longuet-Higgins, M. S., A theory of the origin of microseisms, *Phil. Trans. R. Soc. Lond.*,  
551 *243*, 1–35, 1950.
- 552 Menon, R., P. Gerstoft, and W. S. Hodgkiss, On the apparent attenuation in the  
553 spatial coherence estimated from seismic arrays, *J. Geophys. Res.*, *119*, 3115–3132,  
554 doi:10.1002/2013JB010,835, 2014.
- 555 Mitchell, B. J., Anelastic structure and evolution of the continental crust and upper mantle  
556 from seismic surface wave attenuation, *Rev. Geophys.*, *33*, 441–462, 1995.
- 557 Press, W. H., S. A. Teukolsky, W. T. Vetterling, and B. P. Flannery, *Numerical Recipes in*  
558 *Fortran 77*, Cambridge University Press, 1992.
- 559 Prieto, G. A., J. F. Lawrence, and G. C. Beroza, Anelastic earth structure from the coherency  
560 of the ambient seismic field, *J. Geophys. Res.*, *114*, 2009.
- 561 Romanowicz, B. A., and B. J. Mitchell, Deep earth structure: Q of the earth from crust to  
562 core, in *Treatise of Geophysics, Second Edition*, pp. 789–827, Elsevier, Amsterdam, 2015.
- 563 Snieder, R., Extracting the Green’s function of attenuating heterogeneous acoustic media  
564 from uncorrelated waves, *J. Acoust. Soc. Am.*, *121*, 2637–2643, doi:10.1121/1.2713,673,  
565 2007.
- 566 Strauss, W. A., *Partial Differential Equations*, John Wiley & Sons, 2008.
- 567 Tanimoto, T., Modelling curved surface wave paths: membrane surface wave synthetics,  
568 *Geophys. J. Int.*, *102*, 89–100, 1990.
- 569 Tromp, J., and F. Dahlen, Variational principles for surface wave propagation on a laterally  
570 heterogeneous Earth—III. Potential representation, *Geophys. J. Int.*, *112*, 195–209, 1993.
- 571 Tsai, V. C., Understanding the amplitudes of noise correlation measurements, *J. Geophys.*  
572 *Res.*, *116*, 2011.
- 573 Tukey, J. W., *Exploratory data analysis*, Addison-Wesley, Reading, PA, 1977.
- 574 Viens, L., M. Denolle, H. Miyake, S. Sakai, and S. Nakagawa, Retrieving impulse response  
575 function amplitudes from the ambient seismic field, *Geophys. J. Int.*, *210*(1), 210–222,  
576 doi:10.1093/gji/ggx155, 2017.
- 577 Weaver, R. L., On the amplitudes of correlations and the inference of attenuations, specific  
578 intensities and site factors from ambient noise, *Comptes Rendus Geoscience*, *343*(8), 615–  
579 622, doi:10.1016/j.crte.2011.07.001, 2011.
- 580 Weemstra, C., L. Boschi, A. Goertz, and B. Artman, Seismic attenuation from recordings of  
581 ambient noise, *Geophysics*, *78*, Q1–Q14, doi:10.1190/geo2012–0132.1, 2013.

582 Weemstra, C., W. Westra, R. Snieder, and L. Boschi, On estimating attenuation from the  
 583 amplitude of the spectrally whitened ambient seismic field, *Geophys. J. Int.*, 197, 1770–  
 584 1788, doi:10.1093/gji/ggu088, 2014.

585 Weemstra, C., R. Snieder, and L. Boschi, On the attenuation of the ambient seismic field:  
 586 Inferences from distributions of isotropic point scatterers, *Geophys. J. Int.*, 203, 1054–1071,  
 587 doi:10.1093/gji/ggv311, 2015.

588 Yang, Y., and M. H. Ritzwoller, Characteristics of ambient seismic noise as a source for  
 589 surface wave tomography, *Geochem. Geophys. Geosyst.*, 9, DOI:10.1029/2007GC001,814,  
 590 2008.

## 591 **Appendix A Green’s functions of the scalar wave equation** 592 **(homogeneous lossless media)**

593 We describe in the following two definitions of the Green’s function that are commonly found  
 594 in the literature. In one case (sec. A.1), the Green’s function is obtained by prescribing  
 595 nonzero initial velocity at the source; initial displacement is zero and no other forcing is  
 596 present. In another case (sec. A.4), both initial displacement and velocity are everywhere  
 597 zero, but an impulsive force is applied at the source. Following *Boschi and Weemstra* [2015],  
 598 we adhere throughout this study to the former definition, but in sec. 2.2 implicitly make use  
 599 of the latter. Through the mathematical tools provided in secs. A.2 and A.3, a relationship  
 600 between the two definitions is obtained; this relationship is employed in sec. 2.2.

### 601 **A.1 Green’s problem as homogeneous equation**

602 In analogy with *Boschi and Weemstra* [2015], we call Green’s function  $G_{2D} = G_{2D}(\mathbf{x}, \mathbf{x}_S, t)$   
 603 (with  $t$  denoting time) the solution of

$$\nabla^2 G_{2D} - \frac{1}{c^2} \frac{\partial^2 G_{2D}}{\partial t^2} = 0, \quad (\text{A.1})$$

604 with initial conditions

$$G_{2D}(\mathbf{x}, \mathbf{x}_S, 0) = 0, \quad (\text{A.2})$$

605

$$\frac{\partial G_{2D}}{\partial t}(\mathbf{x}, \mathbf{x}_S, 0) = P\delta(\mathbf{x} - \mathbf{x}_S), \quad (\text{A.3})$$

606 i.e. an impulsive source at  $\mathbf{x}_S$ . Only “causal” solutions, vanishing when  $t < 0$ , are relevant.  
 607 The scalar constant  $P$  serves to remind us of the physical dimensions of  $G_{2D}$ ; for instance, one  
 608 can think of (A.1) as the displacement equation for a membrane, in which case  $\frac{\partial G_{2D}}{\partial t}(\mathbf{x}, \mathbf{x}_S, 0)$   
 609 is the initial velocity, and  $P$  has dimensions of cubed distance over time (recall that, in two  
 610 dimensions,  $\delta$  has dimensions of one over squared distance).

611 *Boschi and Weemstra* [2015] show that, in the time domain, the “Green’s problem” (A.1)-  
 612 (A.3) has solution

$$G_{2D}(\mathbf{x}, t) = \frac{P}{2\pi c^2} \frac{H\left(t - \frac{x}{c}\right)}{\sqrt{t^2 - \frac{x^2}{c^2}}}, \quad (\text{A.4})$$

613 where  $H$  denotes the Heaviside function. This corresponds to

$$G_{2D}(\mathbf{x}, \omega) = \frac{P}{4i\sqrt{2\pi}c^2} H_0^{(2)}\left(\frac{\omega x}{c}\right) \quad (\text{A.5})$$

614 in the frequency domain, with  $H_0^{(2)}$  denoting the zeroth-order Hankel function of the *second*  
 615 kind. When  $\omega x/c \gg 1$ , the expression (A.5) can be replaced by the far-field/high-frequency  
 616 approximation

$$G_{2D}(\mathbf{x}, \omega) \approx \frac{P}{4i\pi c^{3/2}} \frac{e^{-i\left(\frac{\omega x}{c} - \frac{\pi}{4}\right)}}{\sqrt{\omega x}}. \quad (\text{A.6})$$

617 It might be noticed upon comparing our expression (A.5) for  $G_{2D}(\mathbf{x}, \omega)$  with that of, e.g.,  
 618 *Tsai* [2011], that the membrane-wave Green's function given in that study is proportional  
 619 to the zeroth-order Hankel function of the *first* kind: this apparent discrepancy is explained  
 620 by the fact that the Fourier-transform convention assumed by *Tsai* [2011] differs from ours  
 621 (compare eq. (4) of *Tsai* [2011] and eq. (B2) of *Boschi and Weemstra* [2015], and consider  
 622 eq. (E16) of *Boschi and Weemstra* [2015]).

## 623 A.2 Duhamel's principle

624 Consider the initial-value problem

$$\nabla_1^2 u - \frac{1}{c^2} \frac{\partial^2 u}{\partial t^2} = \eta(\mathbf{x}, t), \quad (\text{A.7})$$

$$u(\mathbf{x}, 0) = 0, \quad (\text{A.8})$$

$$\frac{\partial u}{\partial t}(\mathbf{x}, 0) = 0, \quad (\text{A.9})$$

627 with  $\eta$  an arbitrary forcing term. Suppose that a solution  $v(\mathbf{x}, t)$  to the following, similar  
 628 homogeneous problem can be found:

$$\nabla_1^2 v - \frac{1}{c^2} \frac{\partial^2 v}{\partial t^2} = 0, \quad (\text{A.10})$$

$$v(\mathbf{x}, 0; \zeta) = 0, \quad (\text{A.11})$$

$$\frac{\partial v}{\partial t}(\mathbf{x}, 0; \zeta) = Dc^2 \eta(\mathbf{x}, \zeta), \quad (\text{A.12})$$

631 with  $D$  a scalar constant.

632 It can be shown by direct substitution (applying Leibniz's rule for differentiating under  
 633 the integral sign) that if  $v(\mathbf{x}, t; \zeta)$  solves (A.10)-(A.12) for all possible values of  $\zeta$ , and

$$u(\mathbf{x}, t) = \frac{1}{D} \int_0^t d\zeta v(\mathbf{x}, t - \zeta; \zeta), \quad (\text{A.13})$$

634 then  $u(\mathbf{x}, t)$  solves (A.7)-(A.9).

635 This result is known as Duhamel's principle [e.g. *Hildebrand*, 1976; *Strauss*, 2008].

## 636 A.3 General initial condition

637 Once the Green's function associated with a given differential equation is found, it can be used  
 638 to solve rapidly more general initial-value problems based on the same equation. Consider

639 for example

$$\nabla_1^2 f - \frac{1}{c^2} \frac{\partial^2 f}{\partial t^2} = 0 \quad (\text{A.14})$$

640 with the more general initial conditions

$$f(\mathbf{x}, 0) = 0, \quad (\text{A.15})$$

641

$$\frac{\partial f}{\partial t}(\mathbf{x}, 0) = \theta(\mathbf{x}). \quad (\text{A.16})$$

642 It can be proved by direct substitution that if  $G_{2D}$  solves (A.1)-(A.3), then

$$f(\mathbf{x}, t) = \frac{1}{P} \int_{\mathbb{R}^2} d^2 \mathbf{x}' G_{2D}(\mathbf{x}, \mathbf{x}', t) \theta(\mathbf{x}') \quad (\text{A.17})$$

643 solves (A.14)-(A.16).

644 Problem (A.14)-(A.16) is equivalent to (A.10)-(A.12), provided that condition (A.16) is  
645 replaced with

$$\frac{\partial f}{\partial t}(\mathbf{x}, 0; \zeta) = Dc^2 \eta(\mathbf{x}, \zeta). \quad (\text{A.18})$$

646 Then, based on Duhamel's principle,

$$\begin{aligned} u(\mathbf{x}, t) &= \frac{1}{D} \int_0^t d\zeta f(\mathbf{x}, t - \zeta; \zeta) \\ &= \frac{c^2}{P} \int_0^t d\zeta \int_{\mathbb{R}^2} d^2 \mathbf{x}' G_{2D}(\mathbf{x}, \mathbf{x}', t - \zeta) \eta(\mathbf{x}', \zeta) \end{aligned} \quad (\text{A.19})$$

647 solves the general inhomogeneous problem (A.7)-(A.9) for any forcing term  $\eta(\mathbf{x}, t)$ .

#### 648 **A.4 Green's problem as inhomogeneous equation**

649 We next consider the membrane-displacement eq. (5); it is convenient to choose the forcing  
650 term  $U(0, \omega) f(x_1, x_2, \omega) = -i\omega F \delta(\mathbf{x} - \mathbf{x}_S)$  so that  $q = F \delta(\mathbf{x} - \mathbf{x}_S)$  in sec. 2.2. In the time  
651 domain the resulting equation reads

$$\nabla_1^2 u(\mathbf{x}, t) - \frac{1}{c^2} \frac{\partial^2}{\partial t^2} u(\mathbf{x}, t) = -F \delta(\mathbf{x} - \mathbf{x}_S) \delta'(t), \quad (\text{A.20})$$

652 where  $\delta'(t)$  denotes the derivative of the delta function. Assuming zero initial displacement  
653 and velocity, eq. (A.20) is a particular case of problem (A.7)-(A.9). A solution is found by  
654 substituting  $\eta(\mathbf{x}, t) = -F \delta(\mathbf{x} - \mathbf{x}_S) \delta'(t)$  into eq. (A.19),

$$\begin{aligned} u(\mathbf{x}, t) &= -\frac{Fc^2}{P} \int_0^t d\zeta \int_{\mathbb{R}^2} d^2 \mathbf{x}' G_{2D}(\mathbf{x}, \mathbf{x}', t - \zeta) \delta(\mathbf{x}' - \mathbf{x}_S) \delta'(\zeta) \\ &= -\frac{Fc^2}{P} \int_0^t d\zeta \delta'(\zeta) G_{2D}(\mathbf{x}, \mathbf{x}_S, t - \zeta) \\ &= \frac{Fc^2}{P} \frac{\partial}{\partial t} G_{2D}(\mathbf{x}, \mathbf{x}_S, t). \end{aligned} \quad (\text{A.21})$$

655 In the frequency domain, this maps to

$$u(\mathbf{x}, \omega) = i\omega \frac{Fc^2}{P} G_{2D}(\mathbf{x}, \mathbf{x}_S, \omega). \quad (\text{A.22})$$

656 In the literature, problem (A.7)-(A.9) with an impulsive forcing term is often presented as  
657 the Green's problem, and its solution (A.21), (A.22) as the Green's function. It is important  
658 to realize that this is not mathematically the same as our Green's function  $G_{2D}$ . Other defi-  
659 nitions of Green's function likewise exist. In practice, the phrase "Green's function" always  
660 refers to the response of a medium to an impulsive excitation; but this definition is ambigu-  
661 ous, and, for any given medium, the "impulsive response" can be defined mathematically in  
662 a virtually unlimited variety of ways.

## 663 Appendix B Approximate expression for the damped-membrane 664 Green's function

665 We show in the following that, as long as attenuation is weak, the lossy-membrane Green's  
666 function

$$G_{2D}^d(x_1, x_2, \omega) = -\frac{iP}{4\sqrt{2\pi}c^2} H_0^{(2)} \left( x \sqrt{\frac{\omega^2}{c^2} - \frac{2i\alpha\omega}{c}} \right) \quad (\text{copy of eq. 8})$$

667 can be approximated by the product of the lossless Green's function  $G_{2D}$  and a term that  
668 decays exponentially with source-receiver distance. Two different arguments are provided in  
669 the next two sections.

### 670 B.1 Stationary-phase approach

671 If  $z$  is small,  $\sqrt{1+iz} \approx 1+iz/2$  is accurate to first order in  $z$ . It is then reasonable to write  
672 the argument of  $H_0^{(2)}$  in eq. (8)

$$\begin{aligned} x \sqrt{\frac{\omega^2}{c^2} - \frac{2i\alpha\omega}{c}} &= \frac{\omega x}{c} \sqrt{1 - \frac{2i\alpha c}{\omega}} \\ &= \frac{\omega x}{c} (1 - \varepsilon i), \end{aligned} \quad (\text{B.1})$$

673 where  $\varepsilon \approx c\alpha/\omega \ll 1$ .

674 Substituting expression (B.1) into the integral representation of  $H_0^{(2)}$ , e.g. eq. (10.9.11)  
675 of DLMF,

$$\begin{aligned} H_0^{(2)} \left( x \sqrt{\frac{\omega^2}{c^2} - \frac{2i\alpha\omega}{c}} \right) &= \frac{i}{\pi} \int_{-\infty}^{+\infty} dt e^{-i \cosh(t) \left[ \frac{\omega x}{c} (1-i\varepsilon) \right]} \\ &= \frac{i}{\pi} \int_{-\infty}^{+\infty} dt e^{-i \frac{\omega x}{c} \cosh(t)} e^{-\varepsilon \frac{\omega x}{c} \cosh(t)}. \end{aligned} \quad (\text{B.2})$$

676 V. Tsai (personal communication, 2013) first derived eq. (B.2), and solved the integral on  
677 its right-hand side via the stationary-phase approximation. The right-hand side of (B.2) has  
678 indeed the same form as the one-dimensional stationary-phase integral, e.g. eq. (A1) of  
679 *Boschi and Weemstra [2015]*, except for the fact that the non-oscillatory term  $e^{-\varepsilon \frac{\omega x}{c} \cosh(t)}$   
680 depends not only on the integration variable  $t$ , but also on  $x$ . Because this term is small in  
681 the vicinity of the (only) stationary point  $t=0$ , we assume that the stationary-phase formula  
682 still applies; considering that  $\cosh$  coincides with its second derivative, and that  $\cosh(0) = 1$ ,

683 it follows from eq. (A2) of *Boschi and Weemstra* [2015] that

$$\int_{-\infty}^{+\infty} dt e^{-i\frac{\omega x}{c} \cosh(t)} e^{-\varepsilon \frac{\omega x}{c} \cosh(t)} \approx 2 e^{-\varepsilon \frac{\omega x}{c}} e^{-i(\frac{\omega x}{c} - \frac{\pi}{4})} \sqrt{\frac{\pi c}{2\omega x}}, \quad (\text{B.3})$$

684 with the factor 2 at the right-hand side to account for the fact that the stationary point  $t=0$   
685 is *not* one of the integration limits. Consequently,

$$\begin{aligned} H_0^{(2)} \left( x \sqrt{\frac{\omega^2}{c^2} - \frac{2i\alpha\omega}{c}} \right) &\approx \sqrt{\frac{2c}{\pi\omega x}} e^{-\alpha x} e^{-i(\frac{\omega x}{c} - \frac{\pi}{4})} \\ &\approx H_0^{(2)} \left( \frac{\omega x}{c} \right) e^{-\alpha x}, \end{aligned} \quad (\text{B.4})$$

686 where we have replaced  $\varepsilon$  with  $c\alpha/\omega$ . Substituting eq. (B.4) into (8),

$$G_{2D}^d(x_1, x_2, \omega) \approx -\frac{iP}{4\sqrt{2\pi c^2}} H_0^{(2)} \left( \frac{\omega x}{c} \right) e^{-\alpha x} \quad (\text{B.5})$$

687 Importantly, this approximation is only valid for large  $x$ , i.e. the presence of sources in the  
688 near field of the receivers, which is necessary to reconstruct the Green's function according  
689 to sec. 2.2, introduces a possibly significant error.

## 690 B.2 Taylor-series approach

691 Making use, again, of the Taylor expansion  $\sqrt{1+iz} \approx 1+iz/2$  in the argument of  $G_{2D}^d$ ,

$$\begin{aligned} G_{2D}^d(x_1, x_2, \omega) &= -\frac{iP}{4\sqrt{2\pi c^2}} H_0^{(2)} \left( \frac{\omega x}{c} \sqrt{1 - \frac{2i\alpha c}{\omega}} \right) \\ &\approx -\frac{iP}{4\sqrt{2\pi c^2}} H_0^{(2)} \left( \frac{\omega x}{c} - i\alpha x \right). \end{aligned} \quad (\text{B.6})$$

692 If one substitutes into (B.6) the far-field and/or high-frequency approximation for  $H_0^{(2)}$  [e.g.  
693 *Boschi and Weemstra*, 2015, eq. (C5)],

$$G_{2D}^d(x_1, x_2, \omega) \approx -\frac{iP}{4\sqrt{2\pi c^2}} \sqrt{\frac{2}{\pi \left(\frac{\omega}{c} - i\alpha\right) x}} e^{-i(\frac{\omega x}{c} - \frac{\pi}{4})} e^{-\alpha x} \quad (\text{B.7})$$

694 Expression (B.7) can be simplified if one considers that, for small  $z$ ,  $(1-iz)^{-\frac{1}{2}} \approx 1+iz/2$   
695 is accurate to first order in  $z$ ; after so expanding the square root,

$$\begin{aligned} G_{2D}^d(x_1, x_2, \omega) &\approx -\frac{iP}{4\sqrt{2\pi c^2}} \left( 1 + i\frac{\alpha c}{2\omega} \right) \sqrt{\frac{2}{\pi \frac{\omega x}{c}}} e^{-i(\frac{\omega x}{c} - \frac{\pi}{4})} e^{-\alpha x}, \\ &\approx -\frac{iP}{4\sqrt{2\pi c^2}} \left( 1 + i\frac{\alpha c}{2\omega} \right) H_0^{(2)} \left( \frac{\omega x}{c} \right) e^{-\alpha x}, \end{aligned} \quad (\text{B.8})$$

696 and the leading term at the right-hand side coincides with the right-hand side of eq. (B.5).  
697 Let us emphasize, again, that this simplification relies not only on the weak-scattering ap-  
698 proximation, but also on the far-field approximation for  $H_0^{(2)}$ .